

UNCLASSIFIED

AD 400 749

*Reproduced
by the*

ARMED SERVICES TECHNICAL INFORMATION AGENCY
ARLINGTON HALL STATION
ARLINGTON 12, VIRGINIA



UNCLASSIFIED

NOTICE: When government or other drawings, specifications or other data are used for any purpose other than in connection with a definitely related government procurement operation, the U. S. Government thereby incurs no responsibility, nor any obligation whatsoever; and the fact that the Government may have formulated, furnished, or in any way supplied the said drawings, specifications, or other data is not to be regarded by implication or otherwise as in any manner licensing the holder or any other person or corporation, or conveying any rights or permission to manufacture, use or sell any patented invention that may in any way be related thereto.

63-3-1

OFFICE OF NAVAL RESEARCH
Contract Nonr 982-(08)
Task No. NR 051 - 418

FINAL REPORT

THE EFFECT OF SOLID STATE DISLOCATIONS
UPON THE
CATALYTIC ACTIVITY OF METALS

by

T. D. Perkins, C. M. Sliepcevich, and W. R. Upthegrove

University of Oklahoma Research Institute
Norman, Oklahoma

1 March 1963



CATALOGED BY ASTIA
AS AD NO. 400749

400749

Reproduction in whole or in part is permitted for any
purpose of the United States Government.

THE EFFECT OF SOLID STATE DISLOCATIONS UPON
THE CATALYTIC ACTIVITY OF METALS*

ABSTRACT

This report presents the results of an experimental investigation to determine the effect of dislocations upon catalytic activity. The dislocation density, superficial surface area, microscopic surface area, and mass of a silver catalyst were measured, and the (211) plane of the metal subsequently used to catalyze the decomposition of formic acid.

Dislocation densities were varied by deforming plastically the metallic catalyst and ranged from 10^6 to upward of 10^8 line intersections per square centimeter. Decomposition rates for the formic acid reaction were measured over a temperature range of 165 to 190° C and a pressure range of 20 to 70 millimeters of mercury.

The effect of different dislocation densities upon catalytic activity was shown to be related to the change in hydrogen overpotential.

*This report presents the material submitted by T. D. Perkins as a dissertation to the Graduate Faculty of the University of Oklahoma in partial fulfillment of the requirements for the degree of Doctor of Philosophy.

INDEX OF TECHNICAL REPORTS

Report Number	Date
1	15 November 1960
2	15 November 1961
3	15 November 1962

INDEX OF PUBLICATIONS

No publications have been made in connection with the work performed under this contract.

ACKNOWLEDGMENT

The author is indebted to Professors W. R. Upthegrove and C. M. Sliepcevich who helped initiate this research program and who worked closely with the author throughout the course of the investigation.

It is also a pleasure to acknowledge the help of many fellow students, notably Mr. Ben D. Wagner, who assisted in the growth of the crystals, and Mr. Robert G. Rein, Jr., who made the hydrogen overpotential measurements.

For assistance in the design and fabrication of several items of equipment, the writer expresses grateful appreciation to Messrs. James Hood, Norman Alexander, Gene Scott, and John Edmondson of the Physics Shops.

The author further desires to thank the personnel of the Research and Development Department, Continental Oil Company, particularly Messrs. William H. Harwood and Larry Lively, for help in the design of the constant temperature air bath and the chromatograph.

Finally for financial assistance in the form of a fellowship the author wishes to express appreciation to The Ethyl Corporation. And to the Office of Naval Research, whose financial support in part made this investigation possible, the writer is grateful.

Thomas D. Perkins

TABLE OF CONTENTS

	Page
LIST OF TABLES	vii
LIST OF ILLUSTRATIONS	viii
Chapter	
I. INTRODUCTION AND REVIEW OF PREVIOUS WORK	1
II. EXPERIMENTAL EQUIPMENT AND PROCEDURES	8
Growth and Preparation of Silver Catalyst	
Formic Acid Decomposition Reaction Equipment	
Chromatograph	
Operation of the Chromatograph	
Procedure for Reaction Rate Measurements	
Hydrogen Overpotential Measurements	
III. THEORY	34
Hydrogen Overpotential	
Dislocations and Plastic Deformation	
Chemical Reaction Rates	
IV. RESULTS	44
V. CONCLUSIONS	59
REFERENCES	60
APPENDICES	62
A. NOMENCLATURE	62
B. DISLOCATION DENSITY DATA AND SAMPLE DATA SHEET & DISLOCATION DENSITY CALCULATION	65
C. HYDROGEN OVERPOTENTIAL AREA DATA AND SAMPLE DATA SHEET & AREA CALCULATION	68
D. FORMIC ACID DECOMPOSITION RATE DATA AND SAMPLE DATA SHEET & RATE CALCULATION	71

	Page
E. CHROMATOGRAPH CALIBRATION DATA	90
F. EFFECT OF PRESSURE AND TEMPERATURE ON THE DECOMPOSITION RATE OF FORMIC ACID	96
G. ERRORS IN THE DISLOCATION DENSITY AND FORMIC ACID DECOMPOSITION RATE MEASUREMENTS	100
H. CALCULATIONS FOR MASS TRANSFER AND TEMPERA- TURE GRADIENTS IN THE DECOMPOSITION REACTION	102
I. COMPUTED VALUES FOR THE DISLOCATION DENSITY ENERGY AND THE ENERGY OF PLASTIC DEFORMATION	104

LIST OF TABLES

Table	Page
1. Dislocation Density Data	67
2. Hydrogen Overpotential Area Data	69
3. Formic Acid Decomposition Rate Data	89
4. Chromatograph Calibration Data	91
5. Standard Deviations for Dislocation Density Measurements	101
6. Probable Mean Error in Formic Acid Rate Measurements	101
7. Computed Values for the Dislocation Density Energy	105
8. Computed Values for the Energy of Plastic Deformation	105

LIST OF ILLUSTRATIONS

Figure	Page
1. Crystal Growth Equipment	9
2. Glass Reaction System	18
3. Stirring Ring and Seal for Reaction Flask	21
4. Chromatograph Flow Diagram	23
5. Chromatograph Wiring Diagram	24
6. Hydrogen Overpotential Area Apparatus	31
7. Movement on Crystallographic Slip Planes in a Crystal	39
8. Experimental Dislocation Density due to Plastic Bending versus Theoretical Dislocation Density	45
9. Dislocation Etch Pits on an Unstrained Silver Surface	46
10. Variation in the Ratio of Hydrogen Overpotential Area (HOA) to Superficial Area as a Function of Dislocation Density ..	48
11. Temperature Dependence of Catalyzed Decomposition Rate of Formic Acid, Based on Superficial Area	50
12. Temperature Dependence of Catalyzed Decomposition Rate of Formic Acid, Based on Hydrogen Overpotential Area	53
13. Variation of the HOA Ratio with Dislocation Density	55
14. Temperature Dependence of Catalyzed Decomposition Rate of Formic Acid, Based on Hypothetical Active Area	56

Figure	Page
15. Differential Rate Curve for Catalyzed Decomposition of Formic Acid, Run #524B	73
16. Differential Rate Curve for Catalyzed Decomposition of Formic Acid, Run #2524B	74
17. Differential Rate Curve for Catalyzed Decomposition of Formic Acid, Run #3524B	75
18. Differential Rate Curve for Catalyzed Decomposition of Formic Acid, Run #411A	76
19. Differential Rate Curve for Catalyzed Decomposition of Formic Acid, Run #410A	77
20. Differential Rate Curve for Catalyzed Decomposition of Formic Acid, Run #2410A	78
21. Differential Rate Curve for Catalyzed Decomposition of Formic Acid, Run #3410A	79
22. Differential Rate Curve for Catalyzed Decomposition of Formic Acid, Run #422A	80
23. Differential Rate Curve for Catalyzed Decomposition of Formic Acid, Run #2422A	81
24. Differential Rate Curve for Catalyzed Decomposition of Formic Acid, Run #4422A	82
25. Differential Rate Curve for Uncatalyzed Decomposition of Formic Acid, Run #23	83
26. Differential Rate Curve for Uncatalyzed Decomposition of Formic Acid, Run #24	84
27. Chromatograph Calibration Curve for Carbon Dioxide	93
28. Chromatograph Calibration Curve for Carbon Dioxide	94

Figure	Page
29. Chromatograph Calibration Curve for Air	95
30. Effect of Pressure on the Catalyzed Decomposition Rate of Formic Acid	97
31. Variation of Formic Acid Partial Pressure with Reaction Time	98
32. Effect of Temperature on the Uncatalyzed Decomposition Rate of Formic Acid	99

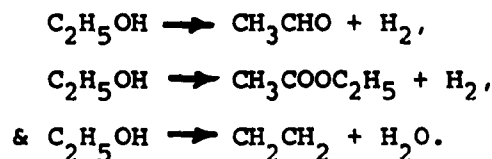
EFFECT OF DISLOCATIONS UPON THE
CATALYTIC ACTIVITY OF SILVER

CHAPTER I

INTRODUCTION AND REVIEW OF PREVIOUS WORK

A catalyst simply increases the rate of a thermodynamically feasible reaction over that obtained in the absence of the catalyst. The catalyst is usually classified according to the function it performs: polymerization, isomerization, alkylation, hydrogenation, dehydrogenation, and so forth.

The primary catalytic function of metals is hydrogenation and dehydrogenation. Metals catalyze these processes by virtue of their ability to adsorb the reactants or products in an appropriate manner. For a given reactant there are sometimes several permissible reaction paths, and the type of catalyst used may determine which path is taken. For example in the decomposition of ethanol over a copper catalyst, possible reactions are:



The first reaction is the favored one, since copper has the ability to adsorb hydrogen rather than water, and further perhaps the ability to adsorb the aldehyde rather than the ether.

For efficient catalysis the strength of adsorption of the reactant(s) must lie within certain wide limits. If a reactant is too strongly adsorbed it will be correspondingly difficult to remove, and it may then constitute a poison. If it is too weakly adsorbed, it will have little chance of remaining on the surface long enough to react.

The notion that the activity of a heterogeneous catalyst resides chiefly at the interface between the solid and the less dense phase has long been held. An atom on the surface is joined by chemical forces to other atoms in the same plane or below it; there is therefore a net resultant force on each surface atom acting toward the bulk. It is this force, or a fraction of it, which acts to adsorb the reactant. In the language of Eyring's Absolute Reaction Rate Theory, the catalyst lowers the potential barrier between reactants and products; or, if one prefers, the catalyst stabilizes the transition state. A second important role which the surface plays is the "activation" of the reactants: for example, the dissociation of molecules into atoms in the hydrogen-deuterium reaction. A third way in which the surface can influence the reaction rate is by bringing the reactants together in a fashion which renders the

formation of a transition state most probable. This statement of course applies to bimolecular reactions.

In principle the constitution of the solid metal may affect the catalytic process proceeding at its surface, and although theoretical descriptions of the surface are of insufficient precision, two somewhat different approaches have been advanced to characterize the bulk metallic state. The Electron Band Theory treats a metal crystal as an assembly of positive nuclei, together with the closed-shell electrons, through which the valency electrons roam more or less freely. With the appropriate application of quantum statistics, this model is used as a basis for deriving electronic properties in terms of the number of valency electrons. The Valence Bond Theory considers the metal crystal as a giant covalent molecule in which each atom is bound to its neighbors by resonating covalent bonds. Cohesive strength and other properties are then described in terms of localized electron orbitals. Each theory has its own merits in explaining the phenomena observed.

For purposes of describing physically the metallic catalyst the usual classifications made are (a) a description of the exposed crystallographic planes, i.e. of the geometry of the perfect arrays of atoms presented to the less dense phase; and (b) a description of the number and nature of surface disorders or defects, i.e. the departure from the ideal conditions assumed in (a). Defects within the bulk

of the solid may be classified according to the number of dimensions in which they exist: (a) point defects, as in the cases of lattice vacancies (Schottky defects) and interstitial atoms (Frenkel defects); (b) line defects, as in the case of dislocations; and (c) plane defects, as in the cases of grain and subgrain boundaries and stacking faults. Point defects may also occur at surfaces, as in the case of the emergence of a dislocation pipe; and one-dimensional defects result when plane defects within the bulk intersect the surface.

The role of surface defects in adsorption and catalysis is difficult to assess. Cratty and Granato (14) point out, in their review of Eckell's work, that the increased activity of nickel for ethylene hydrogenation was of the order of magnitude of the increase in dislocation density produced by cold working the nickel sheet. The value of this observation is diminished by the knowledge that these surfaces were probably contaminated and apparently were not cleaned satisfactorily after being rolled (23).

There is experimental evidence to indicate that defects created by bombardment of surfaces by energetic particles can increase the rates of certain reactions (23, 25). The bombardment of silver by argon ions, followed by a 250° C anneal and subsequent use in the formic acid decomposition reaction, and the bombardment of copper, silver, and copper-silver alloys, followed by various heat treatments, and later

use in the hydrogenation of ethylene, are good illustrations of this behavior. In the former case Sosnovsky ascribed the increase in rate with increasing bombardment voltage to change in the number of dislocation lines intersecting the surface, reasoning that a 250° C anneal prior to the measurements reduced all defects other than dislocations to low numbers.

The suggestion that oxide nuclei might form on dislocations in a metal (8) has been proved wrong by the work of F. W. Young (30) and Coleman and Laukonis (12). Young has shown that boundaries resulting from polygonization in copper do not form rows of oxide nuclei when the oxidation is carried out, unless the dislocations contain impurities (tellurium) in their core. Further he observed a high concentration of random oxide nuclei independent of the polygonization boundaries. Similarly Coleman and Laukonis observed a high density of oxide nuclei during the oxidation of large iron whiskers which did not contain that many dislocations.

Sometimes another factor other than surface preparation of the metal or defect structure obscures chemisorption and catalytic data. Hall and Emmett (16) list many contributors to experimental evidence showing that dissolved hydrogen can modify the activity of metal catalysts.

Gwathmey and Lawless (15) have summarized the findings of Menzel and Menzel-Kopp, who subjected (001) and (111)

planes of silver to oxidation at pressures up to 100 atmospheres, oxygen at temperatures from 200 to 370° C, and for a period of time up to 9 hours. No mechanical or chemical polishing or further anneal was made on the crystals following their growth. The objectives were to study the oxidation on preferential planes and the nature of the oxide film formed. It appears well established that orientation influences adsorption and catalytic phenomena, although two other factors in particular have a strong influence on the processes: the presence or absence of contaminating materials and the topography of the metal surface.

Sosnovsky (22) reported a variation in activation energy with crystal orientation for the silver-catalyzed formic acid decomposition. Wilson, et al (27) found no significantly different results with various silver planes in the catalytic oxidation of ethylene to ethylene oxide with air.

The reactivities of metal powders in terms of hydrogen evolution in dilute acid solutions in the absence of air were determined by Wang and Hackerman (26). Stainless steel, nickel, and chromium powders were prepared by reduction in hydrogen and by limited adsorption of carbon monoxide and oxygen. The chemisorbed carbon monoxide or the sorbed oxygen altered only the induction period and left unchanged the ultimate rate of dissolution.

Findings for hydrogen evolution during electrolysis, or hydrogen overpotential, have been extensively represented

in the literature (2, 4, 5, 6, 7). The chief value of the method lies in the determination of relative areas for metal electrodes, although there has been much controversy over the nature of the rate-limiting step and the values of the constants involved. To an approximation the area obtained by the method may be compared with that measured by adsorption studies with nitrogen gas (2). Measurements may be interpreted as an adjunct to catalytic rate data in providing a dynamic model with which to characterize the surface.

Thus with a view toward defining the influence of one type of metallic line defect, the dislocation, this research was undertaken.

CHAPTER II

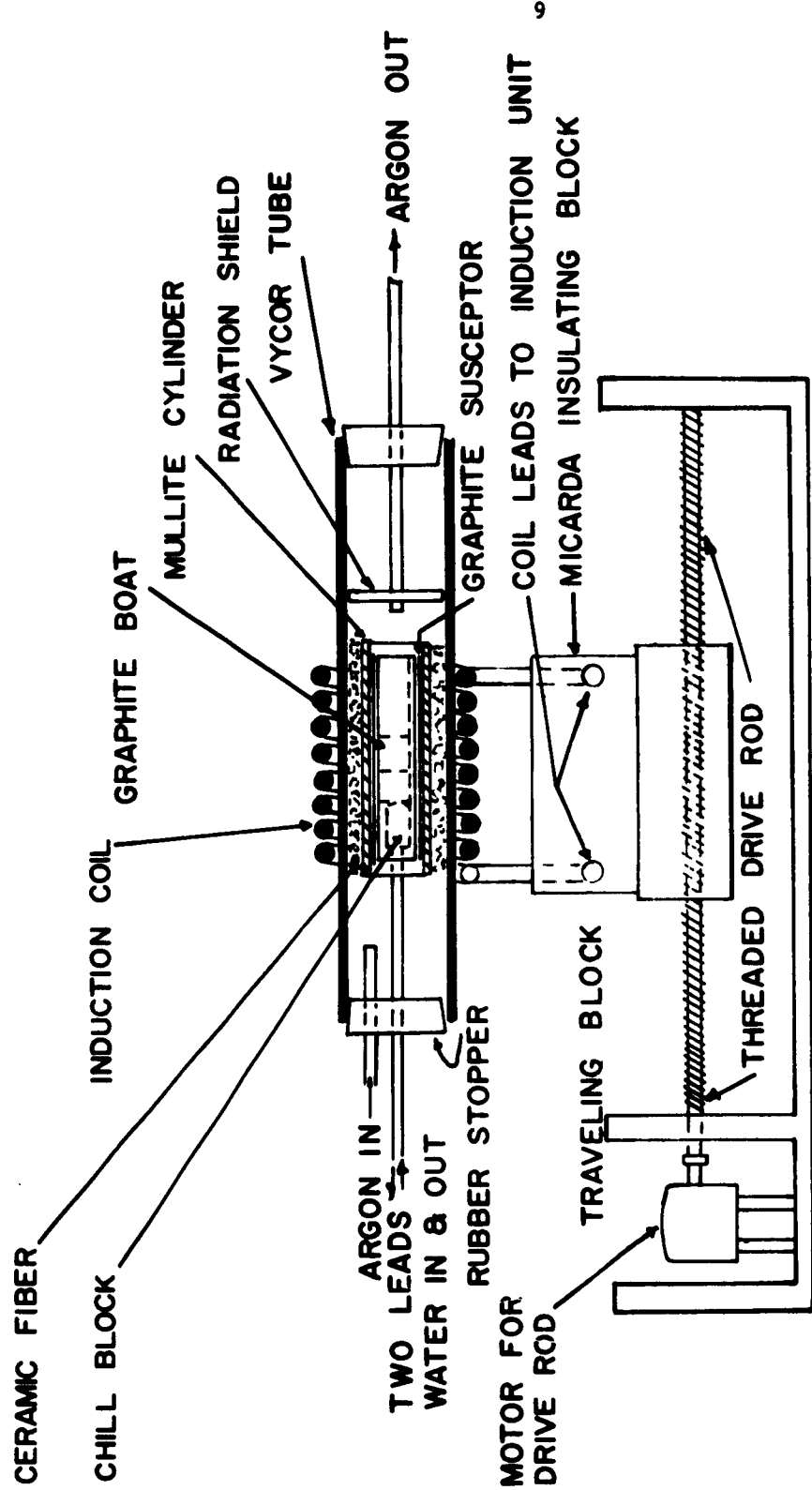
EXPERIMENTAL PROCEDURES AND EQUIPMENT

Experimental investigation involved the growth of single crystals, orientation of these crystals by the Laue X-ray back reflection technique, electropolishing of the silver specimens, thermal etching to delineate dislocation line intersections with the metallic surface; measurement of the hydrogen deposited on the silver surfaces in a platinum-standard hydrogen-silver electrode cell, and measurement of the total pressure, temperature and quantities of materials produced in the silver-catalyzed, formic acid decomposition reaction. The necessary items of procedure and equipment for these operations are the subject of this chapter.

Growth and Preparation of Silver Catalyst

Granular silver of 99.997 per cent purity and bar silver of 99.999 per cent purity were used to produce controlled orientation metallic single crystals by a modified Chalmer's technique (10, 11).

Figure 1 illustrates the equipment necessary for the crystal growth. The boat (or mold) for melting the metal was machined from high density, AUC grade graphite rod. The boat



CRYSTAL GROWTH EQUIPMENT (NOT TO SCALE)

FIGURE 1

front was shaped to receive a brass chill block, 1-inch long by 3/8-inch high by 3/4-inch wide, through which water circulated during the growth process. A steel pin held the chill block in place. The "seed"--piece of single crystal needed to initiate controlled orientation growth--fitted into the channel directly behind the chill block and pressed firmly against the block for good heat transfer. In fact it was necessary to solder the seed to the chill block with silver solder to obtain sufficiently good contact. The seed was about 1-inch long, had a 1/4-inch by 1/4-inch square cross section. The width of the boat increased from 1/4-inch back of the seed channel to 1 1/4-inches at a point 1 1/2-inches further to the rear. There the boat assumed the dimensions of 1 1/4-inches in width by 9/16-inch in depth for a length of 3 1/2-inches. The boat sides were 1/8-inch, while the boat bottom was 3/16-inch. Surrounding the boat was a cylindrical susceptor, 1 11/16-inches I.D. by 1 15/16-inches O.D. by 7-inches long, machined from the same graphite as the boat. A mullite protection tube measuring 2-inches I.D. by 2 1/4-inches O.D. by 10-inches long fitted over the susceptor. Loosely packed fibrerax ceramic bulk fiber was used to center the susceptor in a 3-feet long, 2.76-inch O.D. Vycor tube. The Vycor tube was stoppered on both ends to maintain a dynamic atmosphere of argon gas. An aluminum radiation shield was placed about 3-inches to the rear of the boat. Leads were introduced for water to circulate through the

chill block and for argon gas to flow through the tube. The induction coil of 3/16-inch copper tubing had 7 turns, a 3-inch I.D., and a pitch between turns of about 1/8-inch. It was connected to flexible furnace leads. A 10-kilowatt Lepel radio frequency generator, Model T-10-3, furnished the energy for melting the metal. The induction coil was mounted on a 1/2-inch thickness of Micarta attached to a stainless steel block. The block was tapped to move on a threaded drive rod powered by an electric motor at varying speeds from 1.25 to 15.00-millimeters per minute.

The normal procedure was to charge the mold with about 210-grams of silver, position the boat in the Vycor tube, and purge the tube for 10 minutes with argon. Water flow through the chill block was then started, and heat was supplied to the susceptor and mold by induction from the radio frequency coil. The coil was positioned so as to melt about 1/8-inch to 1/4-inch of the seed (in addition to the metal charge), after which the coil was electrically driven to the rear of the boat at a speed of 4 to 5-millimeters per minute. Solidification of the metal initiated in the seed channel and proceeded toward the boat end. The silver solid-liquid interface usually was concave to the boat front as desired (11). The coil was stopped at the boat end, the heat supplied reduced by some 20 to 30 per cent, and freezing continued to completion. Argon flow continued at 30 to 55-milliliters per minute for some 10 minutes after the heat supply

was terminated. About 50 minutes elapsed during the growth process; a single crystal 5-inches long by 1 1/4-inches wide by 1/4-inch deep was produced.

The silver crystal was removed from the boat and allowed to cool to ambient temperature, after which it was immersed for 1 to 2 minutes in a one part ammonium persulfate, one part sodium cyanide solution to delineate spurious grain formation (19). These chemicals were ACS, Reagent Grade. If the chemical etch outlined no spurious grains, the lattice orientation was determined by interpretation of the Laue X-ray back reflection film, which also served to reveal any small degree of misorientation between lineage subgrains. Insofar as possible crystals were grown with the [211] direction lying in the horizontal plane perpendicular to the growth direction, and with the ($\bar{1}11$) plane making an angle of approximately 45° with the growth direction.

The metallic single crystal was cut into strips approximately 1-inch long by 1/4-inch wide by 1/4-inch deep to expose the (211) plane as the major surface and provide additional surface area for catalyzing the formic acid decomposition. This step was accomplished with a standard water cooled, abrasive cutoff machine. A blade 0.020-inch thick gave the best cutting results.

When the desired orientation was not obtained in the as-grown crystal surfaces, the metal was partially mounted in Koldmount, again X-rayed and oriented to verify the

mounting position in space. Then the metallic crystal was totally encased in the semitransparent material so that the desired planes were either parallel or perpendicular to the macroscopic Koldmount surfaces and presented the preferred orientation for bending.

Cutting distortion was eliminated by mechanical polishing with number 1 and number 00 emery paper followed by electrochemical removal of 0.01-inch of metal in 5 per cent (by weight) solution of potassium cyanide in distilled water. A Beuhler Company electropolisher furnished the control elements for the electropolishing technique. Silver was made the anode for the cell, and a stainless steel beaker served as the cathode. Abrahams has aptly prescribed the conditions for good electropolishing results with silver: (a) fresh solution, (b) current density near 1-ampere per square centimeter, and (c) agitation of specimen by hand at 2 to 3 cycles per second (1). Electropolishing yielded a clean, macroscopically flat surface, free from microscratches and distortion, as revealed by examination under a microscope at 300X. The electropolisher also functioned as an etching apparatus when the current density was 0.1-ampere per square centimeter.

Surface preparation of the silver completed, the metal was subjected to a thermal etch for evaluating the dislocation line intersections present (17). The etching chamber was a 1 3/4-inch O.D., number 304 stainless steel tube, 36-inches long, with a 16-gauge steel shelf extending, at a

height of 1/2-inch, from the tube front backward for 34-inches. The tube end was sealed by a weld of 16-gauge steel plate; a 3-inch O.D. flange was welded to the tube front. The cover flange had two lengths of 1/4-inch O.D. steel tubing welded to it, one 34 1/2-inches long for gas entry to the back of the shelf, and one 3-inches long for gas exit. Inert gas, argon, entered the longer tubing piece, passed over the shelf containing the specimens, and exited through the shorter tube under a pressure of 2 to 3-inches of water. A conventional tube furnace with a Wheelco Amplitrol controller coupled to a chromel-alumel thermocouple maintained the temperature at $600^{\circ} \text{C} \pm 15^{\circ} \text{C}$.

The etching tube was brought to 600°C , a lava boat bearing the specimens inserted, and the tube purged with argon (99.999 per cent minimum purity) for 10 minutes. The argon flow was then reduced to 5 to 15-milliliters per minute, and the specimens maintained at temperature for 30 minutes. The argon flow was then terminated, the etching mixture introduced at rates of 200 to 300-milliliters per minute for the first 3 minutes and 5 to 15-milliliters per minute for the next 7 minutes. The etching mixture flow was halted and argon flow again introduced. Heat supply to the furnace was stopped, and the tube allowed to cool in the inert atmosphere to ambient temperature. The silver specimens normally were bright upon their removal from the tube. Etch pits were counted by viewing the surfaces at 1000 to

2000X magnification on the screen of a well-calibrated Reichert metallograph. A Polaroid camera, mountable on the metallograph screen, facilitated the counting.

Superficial areas of the specimens were measured with a Scherr Microprojector at a magnification of 10X. Electro-polishing followed this measurement when necessary. A standard balance, calibrated to 0.1-milligram, was used to weigh the metal. Ends and edges of the strips were masked with a 0.007-inch fiberglass tape with a silicone polymer adhesive. The tape was pressure and temperature sensitive.

Excess dislocation densities were obtained by simply bending the metal strip to an appropriate radius, 1.32 or 4.00-centimeters, by forcing an aluminum plunger down on the silver, placed in a die of the same material. Initially a teflon die-and-plunger combination was used, but the material proved too soft for uniform metal deformation. During deformation the crystal was constrained so that bending occurred about the [211] direction. Thus the excess dislocation lines produced were perpendicular to the prepared surface and extended through the depth of the crystal specimen.

When bending was done, electropolishing followed to eliminate scratches and prepare the surface for thermal etching treatment. Another means provided for deforming plastically the silver was a hand-rolling mill, adjustable for thicknesses up to 0.28-inch. Roll diameters were 1.965-inches. Care was taken to feed the material through the mill with the same orientation upon each pass.

Equipment and Procedures for the Formic
Acid Decomposition Reaction

An air furnace provided a constant temperature environment for the catalyzed reaction. The temperature controlled space was bounded by a 16-gauge steel shell, 24-inches long by 16-inches wide by 20-inches high, fabricated by the Boardman Company, Oklahoma City, Oklahoma. The shell top was fastened to the sides by means of screws and wing nuts, and it had an opening for access to the interior. A 3/4-inch lip around the circumference of the shell rested on a 3/4-inch thick plywood shelf which supported the inner steel shell. This shelf was attached to the outer 3/4-inch plywood box measuring 30 1/2-inches long by 22 1/2-inches wide by 26 1/2-inches high on the interior. These dimensions provided for a 3 1/4-inch thickness of fiberglass insulation between the steel and plywood shells.

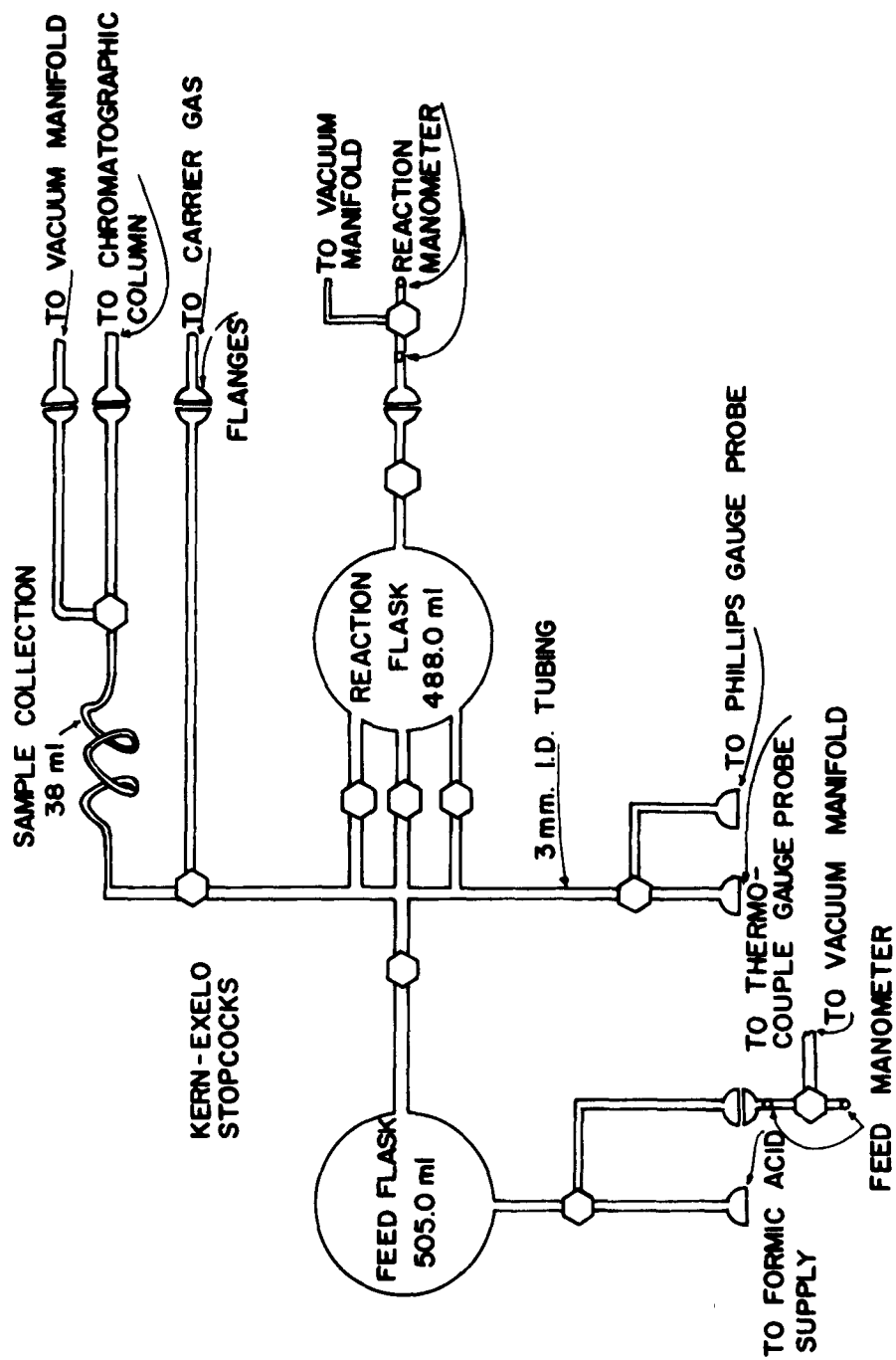
Two 7-inch diameter fans with 1/150-HP motors were mounted in the steel shell; one was placed 6-inches from the shell top on one side, while the second was located 6-inches from the shell bottom on one end. These provided for random mixing of the air and eliminated any substantial gradients within the shell. Each fan shaft passed through two single-shield bearings mounted in either end of a 1-inch O.D. tube which bridged the space between the steel and wood shells. The shaft tube was threaded on either end and secured in place by lock nuts. Molybdenum disulfide grease provided satisfactory lubrication for the shafts and bearings.

Heat for the furnace came from four 250-watt infrared lamps and a 69-ohm, 177-watt resistance wire (chromel A, B&S gauge 30). Two lamps were situated in the steel shell top, and two were located in the shell bottom. They were so connected that one top lamp at one end and one bottom lamp at the opposite end formed a set. Both sets of 500-watts were connected to variable transformers; only one set was required to maintain the control temperature.

A Sargent Model T, electronic temperature sensing and controlling instrument, maintained the selected temperature to within $\pm 0.1^{\circ}$ C. A 177-watt resistance wire heater was connected to this on-off temperature controller, which utilized a thermistor as the sensing element.

Figure 2 outlines the all glass reaction system, located within the air furnace. Tubing diameter was 3-millimeters, except 1/2-inch long leads from the stopcocks and flanges, the sample collection coil, and the carrier gas inlet. These were 9-millimeters O.D., 7-millimeters I.D. The feed and reaction flasks were nominally 500-milliliter Pyrex flasks, modified in the following fashion. The feed reservoir was stoppered with a 24/40 N o-ringed cone sealed off at one end. The reaction flask neck was N size 34/45-socket to accommodate the stirrer and catalyst. A vertical 5/16-inch diameter thermocouple well extended downward to within 1/4-inch of the catalyst surface.

The Kern-Exelo stopcocks consisted of two parts: the lower part, to which were fused tubing leads, and the upper



GLASS REACTION SYSTEM (NOT TO SCALE).

FIGURE 2

part, in which a 3-millimeter bore was fashioned for 180° of the horizontal plane. The two parts were fastened together with screws, nuts, teflon washers, and lock washers. Three tubing leads could be opened simultaneously to one another with the 3-way cock, two with the 2-way cock. Dow-Corning silicone vacuum grease lubricated the ground glass stopcocks. Aluminum sockets fitted over the cocks and received reach rods for rotation from outside the furnace.

The glass flange joints had 7-millimeter I.D., 10-millimeter O.D. stems, used a 7/16-inch I.D., 3/8-inch O.D. Viton o-ring. A size number 18 screw clamp compressed the o-ring between the joints. A thin film of vacuum grease applied to the o-ring helped to make a good vacuum seal.

Precision glass tubing, 1/4-inch I.D., formed the manometer legs for two manometers located exterior to the plywood shell. Triply distilled mercury was the manometric fluid; two or three drops of Octoil covered the mercury surfaces to preclude contamination of the metallic fluid and decrease the vapor pressure. A 3-way stopcock connected between manometer legs provided a means of evacuating either leg with a vacuum pump, admitting air, or completely isolating the manometer. The manometers were mounted on 3/8-inch plywood, faced with glass mirrors to avoid errors of parallax in sighting the readings. Meter sticks were positioned between the legs with Elmer's Glue-All.

A Model 1392 vacuum pump combination, mechanical pump and oil diffusion pump, was capable of producing

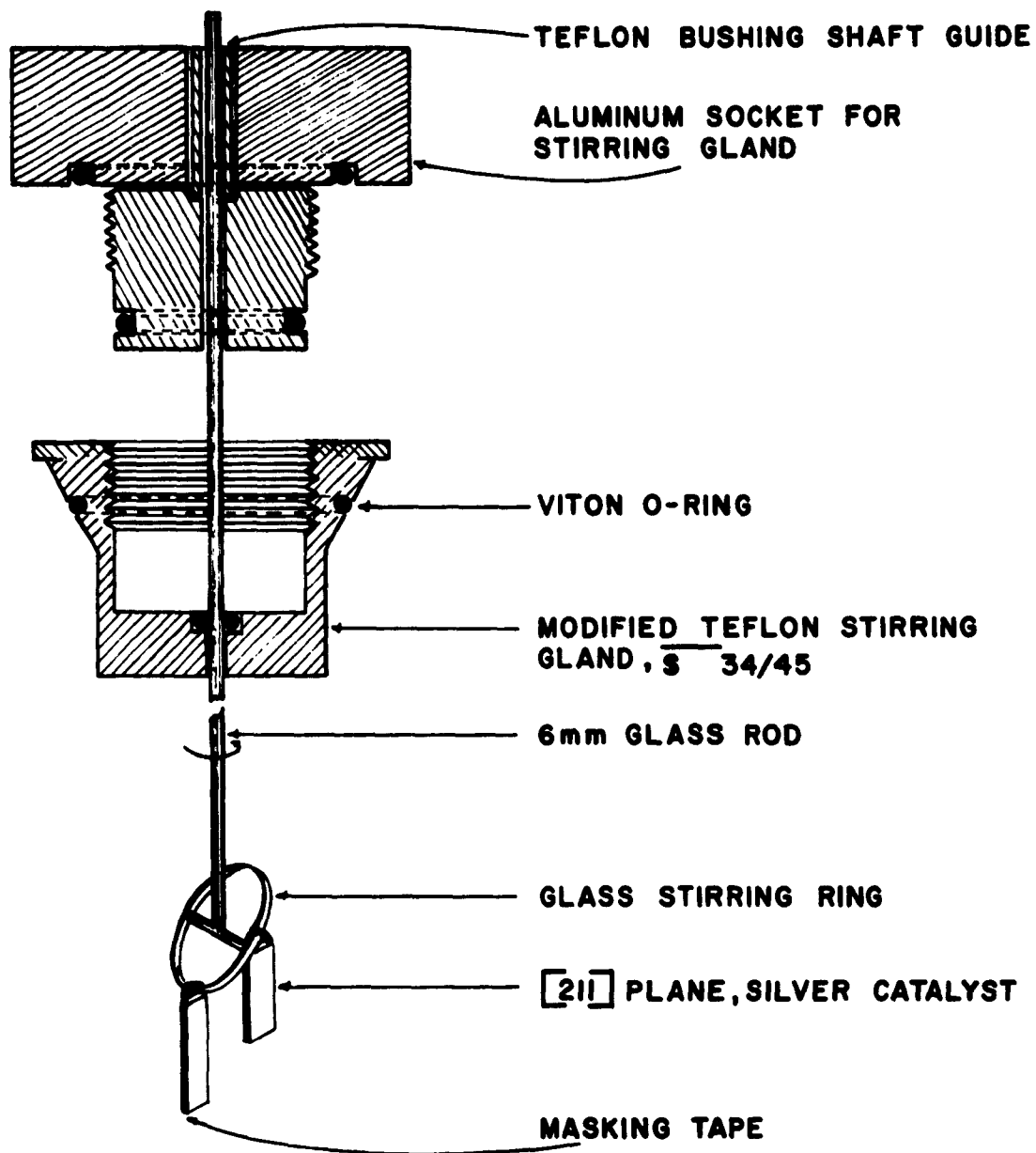
0.001-micron ultimate vacuum. This combination was connected to a glass manifold by means of a corrugated brass bellows, 1 1/8-inches O.D. by 3/4-inch I.D. by 22 corrugations, and sealed with soft solder, Apiezon "W" hard wax and glyptal, high vacuum sealant. The pumps were mounted on cup type vibration mounts, 10-20 pound load range, which together with the flexible bellows, held mechanical vibration transmitted to the glass system within safe limits. Connecting the bellows and vacuum manifold was a cold trap.

A model PGH-T-01 combination thermocouple-Phillips gauge with triple range: 0.01 to 0.1-micron, 0.1 to 5.0-microns, 10 to 1000-microns, measured the vacuum attained within the system. Above 1-millimeter Hg the manometers indicated the existing pressure.

Formic acid, 98 per cent plus HCOOH, high purity grade, was alternately vacuum distilled and solidified three times with dry ice-methanol solution to yield a purified solid with a melting point of 47° F. Prior to distillation the acid was agitated for three days with anhydrous oxalic acid, ACS reagent grade, by using a magnetic, teflon-coated stirring bar.

Catalyst strips were suspended from a Pyrex glass stirring ring 5/8-inch in diameter by means of fiberglas tape, as depicted in Figure 3. A standard 34/45 teflon stirring gland was tapped to receive a threaded aluminum socket bushing having an inner teflon bushing guide. Viton o-rings

21



STIRRING RING & SHAFT SEAL FOR REACTION FLASK
(NOT TO SCALE)

FIGURE 3

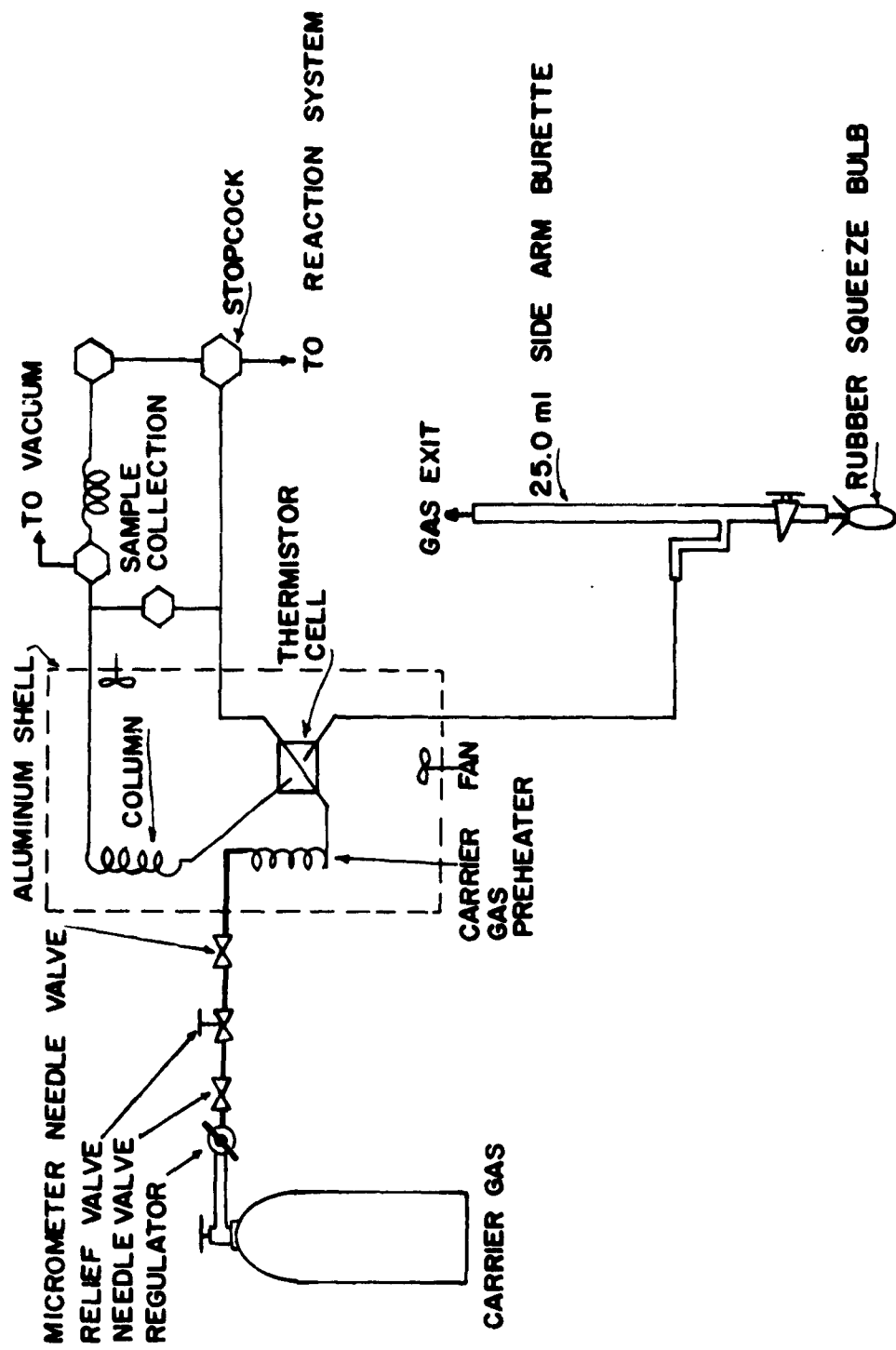
were placed as shown. Drive for the stirring ring came from a variable speed, constant torque, cone drive stirrer. Speed capability ranged from 125 to 500 revolutions per minute.

A calibrated number 20 gauge, type J, iron-constantan thermocouple inserted in the flask well was connected to a Rubicon Model number 2732 portable potentiometer for temperature measurement. The matched thermocouple wires, test number 44320-56162, were obtained from Minneapolis-Honeywell Regulator Company; the estimated accuracy of the calibration curve from 0 to 900° F was $\pm 2^\circ$ F. Over the range of potentials measured, 0 to 16.1-millivolts, the Rubicon instrument was accurate to within 0.005 to 0.013-millivolts (or about 0.3° F).

Chromatograph

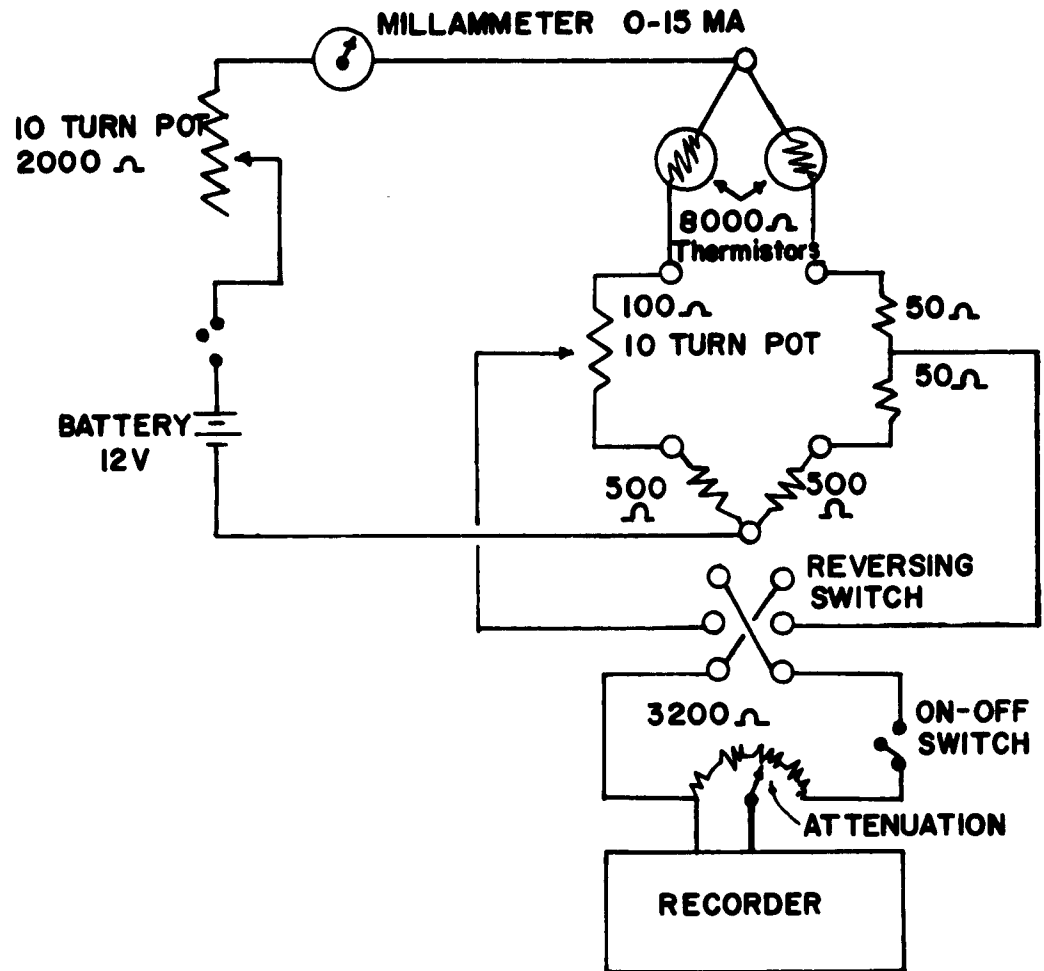
Analysis of reaction products was accomplished by means of vapor phase chromatography, for which sketches of the flow and wiring components are shown below in Figures 4 and 5.

Helium carrier gas, 99.99 per cent minimum purity, flowed through a two-stage regulator, needle valve, 50-pound relief valve, and micrometer needle valve on its way to the 10-foot, 1/4-inch O.D., copper tubing gas preheater. It continued its flow through the reference side of the thermistor cell on the way to purge the sample from the sample collection coil or to bypass the coil. The gas (or gas mixture) continued its flow through the adsorbent column, thence to the sample side of the thermal conductivity cell, and finally



CHROMATOGRAPH FLOW DIAGRAM

FIGURE 4



CHROMATOGRAPH WIRING
FIGURE 5

through the burette, where the rate was measured by following the time of rise of a soap bubble through the 25-milliliter volume with a stopwatch. The gas then exited to the atmosphere.

The thermal conductivity cell contained a matched pair of 8000-ohm thermistors, whose resistance varied inversely with an increase in temperature. Since the thermal conductivities of gases differ, more heat was either extracted or added to the sample thermistor than to the reference thermistor, causing an electrical unbalance in the bridge circuit (see Figure 5). This potential unbalance fed current through the attenuator and caused an appropriate signal to be traced by the recorder pen.

The column consisted of two feet of 1/4-inch O.D. copper tubing rather loosely packed with medium activity charcoal adsorbent. Packing was accomplished by using an aspirator to create a vacuum on one end of the coil. The packing exhibited a different affinity for each of the gases present in the mixture, causing them to be desorbed at different times from the column.

The attenuator provided a means of varying the signal sent to the 1-millivolt range recorder. It consisted of 1/4 per cent tolerance resistors arranged on a non-short-circuiting rotary switch so that the resistance varied in discrete steps by a factor of 2, in a range from 1 to 512.

The recorder was a d-c millivoltmeter Bristol Dynamaster, Model 1PH560-51-T24-T38-T71-T13. Two ranges of

potential could be recorded: -0.05 to 1.05-millivolts and -0.25 to 5.25-millivolts. The automatic standardization feature was modified by inclusion of an on-off switch to prevent standardization during operation of the instrument.

The aluminum shell, insulated by Fibrerax ceramic paper on the inside, housed the preheater, column, and cell in a constant temperature environment of 212° F. This temperature was selected to avoid condensation of water vapor arising from the competing reaction in the formic acid decomposition. Two fans, having four 2 1/2-inch diameter blades and a speed of 2400 revolutions per minute, served to circulate the air and maintain a constant temperature within the walls. One was placed high on a side, the other low on an end to insure random mixing as in the larger air furnace.

Control and ballast heaters of 250 and 300-watts, respectively, were constructed of chromel-A resistance wire to supply heat for the cell and column air bath. They were connected to a model S, thermistor actuating and controlling instrument. The device was of the proportional power input type, capable of sensing and maintaining the selected temperature to within $\pm 0.01^\circ$ C. A conventional 76-millimeter immersion thermometer, -4 to 230° F range, was always immersed to the same depth in the bath to monitor the temperature. No deviation greater than 0.4° F was ever detected from the 212° F temperature reading.

Calibration of the chromatograph consisted of recording the signals for known quantities of gases--hydrogen,

nitrogen-oxygen (air), carbon dioxide, and carbon monoxide-- at various carrier gas flow rates. Cell and column temperatures were constant at 212° F. A 99.205 per cent carbon dioxide, 0.795 per cent carbon monoxide mixture aided in the calibration. Calibration data are given in Appendix E, Figures 27, 28, and 29.

Operation of the Chromatograph

Carrier gas flow was started at least one hour before an analysis was desired. At the same time heat was supplied to the air bath. The recorder was turned on about 30 minutes prior to an analysis and standardized each day. When gradients ceased to exist in the air bath, the carrier flow was adjusted to some 75-milliliters per minute. Battery voltage was maintained at 12-volts ± 0.1 -volt. Current supplied to the thermistor bridge was always 10-milliamperes ± 0.05 -milliampere. Very fine adjustment of the current was possible because of the sensitivity of the 2000-ohm, 10-turn potentiometer and the low demand imposed upon the storage battery. Similarly the 100-ohm, 10-turn rheostat made fine adjustment of the recorder pen to zero deflection possible. Chart speed was always maintained at 3/4-inch per minute and the recorder range at 1.0-millivolt. The reversing switch provided a way of recording a positive peak for hydrogen; unfortunately however the thermal conductivities of hydrogen and helium were very nearly the same at 212° F, resulting in practically no deflection of the recorder pen for hydrogen.

For operation the bridge current was adjusted to 10-milliamperes, and the recorder pen zeroed. The sample collection coil, having first been evacuated to a fraction of a micron, was allowed to fill with sample. The coil was then isolated; the carrier bypass stopcock closed; and the helium flow admitted to the collection coil. Immediately afterwards the stopcock downstream of the coil was opened to provide an uninterrupted flow path for the gas to the column, cell, and burette. Carrier flow rates were measured with a stopwatch readable to 0.05-second and manually recorded on the strip chart. As the various components were eluted from the column and passed through the cell, the recorder pen deflected for a distance and a time proportional to the quantity of component present. Air was first eluted, followed by carbon monoxide and then carbon dioxide.

Since the sample coil pressure (about 50-millimeters Hg) was substantially below the carrier line pressure (about 870-millimeters Hg), a sudden decrease in line pressure accompanied the admittance of carrier gas to the coil. Initially this condition of slight vacuum caused air to be drawn into the carrier line, but later was overcome by insertion of 15-feet of 3/8-inch O.D. copper tubing into the line upstream of the sample collection coil. Thus the carrier flow rate varied during a sample analysis; however there was little variation between flow rates of different samples at comparable times in the analysis sequence.

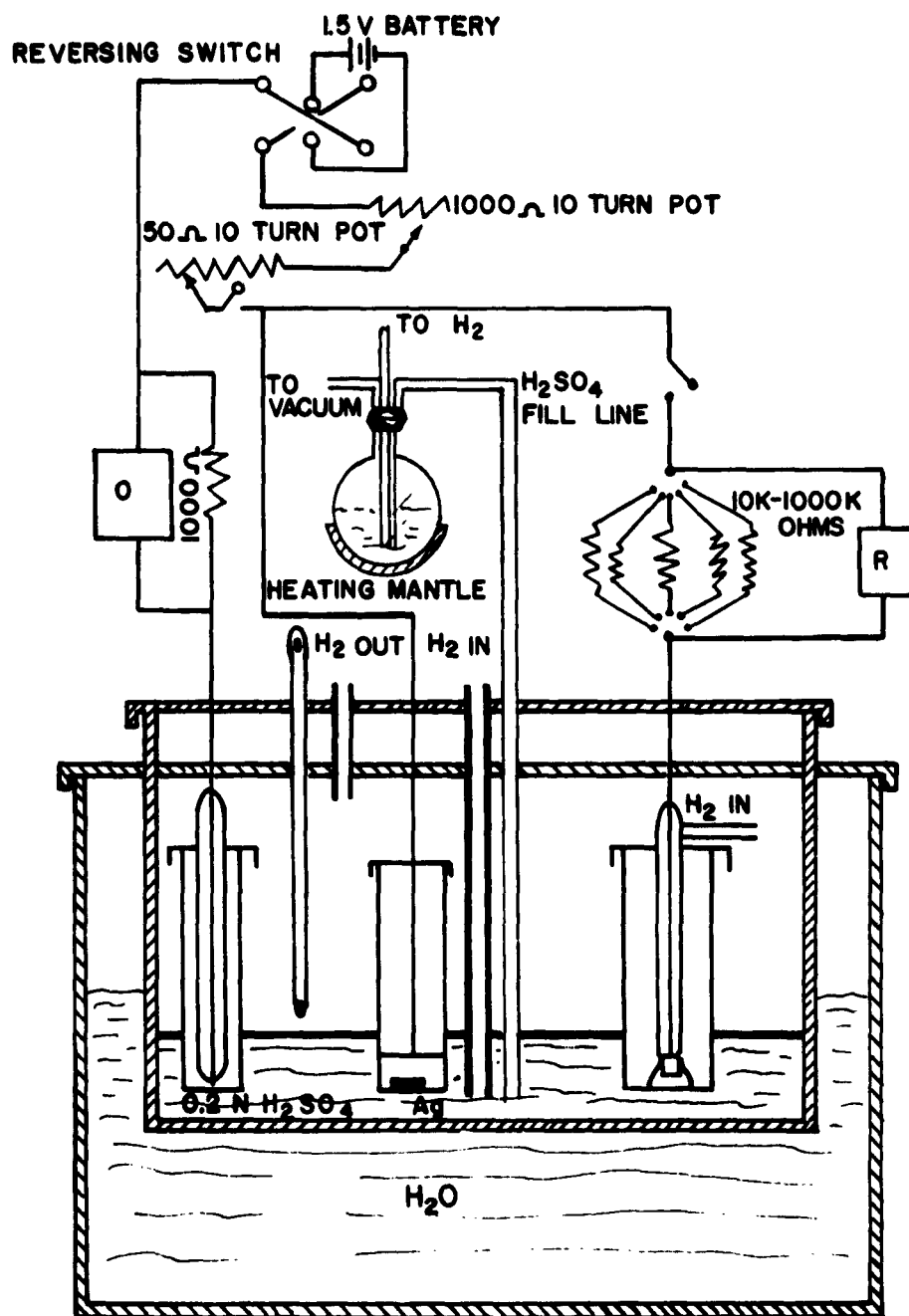
Procedure for Reaction Rate Measurements

The silver catalyst strips were suspended from the glass stirring ring, previously described, and lowered into the reaction flask. The entire system was evacuated to a fraction of a micron and left overnight. The following morning, the system was again evacuated and purified formic acid vapor admitted to the feed flask (Figure 2). Heat was supplied to the air furnace with continuous evacuation of the system, exclusive of the feed flask. Usually the control temperature was reached in 1 1/2 hours, after which this temperature was maintained for 2 to 3 hours to insure steady state conditions and preheat the feed to reaction temperature. When transient temperatures were eliminated, the reaction flask was isolated and formic acid was admitted to the stirred reaction flask. The initial temperature and total pressure were recorded, and a sample of the feed was analyzed with the chromatograph. At intervals of 1/2 to 2 hours samples were taken from one of the three sample lead heights for analysis, and the total pressure was noted on the manometer adjacent to the reaction flask. Temperatures were recorded at more frequent intervals and were measured by the iron-constantan thermocouple and immersion thermometer. The deviation of temperature with time for each device was usually less than 1 1/2° F. The reaction proceeded in batch fashion for 5 to 10 hours. Three or four measurements were made without stirring to test the effectiveness of heat and mass transfer to and from the catalyst.

The data obtained were temperature of reaction, total pressure, amount of each component present, all as a function of reaction time.

Hydrogen Overpotential Measurements

The hydrogen overvoltage apparatus shown in Figure 6 was patterned after that described by Butler (7). A 1.5-volt drycell supplied current for the electrochemical cell comprised of three electrodes: (a) conventional platinum electrode, (b) silver test specimen, and (c) standard hydrogen electrode, modified Hildebrand type. A 50-ohm, 10-turn potentiometer with microdial and a 1000-ohm, 10-turn rheostat with microdial were utilized for coarse and fine adjustments of the potential applied to the electrodes. The reversing switch permitted hydrogen overvoltage decay to be studied. Resistances were selected to allow microamperage flow through the platinum and silver electrodes and almost negligible flow through the hydrogen electrode (i.e. 10^{-9} amperes). One channel (marked O in the sketch) of a Sanborn Twin-Viso Recorder, Model 60-1300, traced the current flow through the platinum electrode. A Model 503, Tetric oscilloscope designated R in the sketch) followed the potential existing between the silver and hydrogen electrodes, and a Dumont oscilloscope camera recorded the trace for permanent record, thereby furnishing a means of detecting the presence of dissolved oxygen or other impurities in the electrolyte (6, 7). The circuitry was so arranged as to trigger the pulse simultaneously upon closing the reversing switch.



HYDROGEN OVERVOLTAGE APPARATUS (NOT TO SCALE)

FIGURE 6

The silver contact wire was soft soldered to the silver test piece and the combination embedded in Koldmount, except for the (211) surface. Since the semitransparent resin cured in the Nalgene plastic cylinder, a good airtight seal was obtained. Cylinder dimensions were 1 1/2-inches O.D. by 4-inches high; friction fit covers protected the contents from contamination. The same cylinders also housed the other two electrodes; the bottoms were perforated with 15 to 20 holes made with a straight pin to obtain good electrical continuity within the electrolyte. The three electrode containers were tightly pressfitted into a 1/4-inch thick teflon plate, which was in turn tightly fitted into the surrounding Nalgene jar. The electrodes were spaced at 120° intervals on a radius of 1 1/4-inches. The smaller jar, 5-inches O.D. by 8 inches high, was placed in another larger cylinder, 7-inches O.D. by 9-inches high, which functioned as a constant temperature water bath container.

Reagent grade sulfuric acid solution was purified by warming for 2 to 3 hours with hydrogen gas bubbling through the mixture under a slight vacuum created with an aspirator. Hydrogen gas, 99.99 per cent minimum purity, passed through a Deoxo unit on its way to the sulfuric acid supply flask, to the standard electrode, or to the electrolyte in the cell. By adjustment of pinch clamps on the supply lines, appropriate hydrogen gas flow to each point was maintained. Gaseous hydrogen leaving the cell passed first to a 250-milliliter

overflow flask, thence to a 250-milliliter "water-bubbler" flask.

Prior to insertion in the cell, the silver had undergone the same preparation mentioned earlier. It was then made cathodic in the same electrolyte used in the cell for further cleaning immediately before the overvoltage measurement. Washing with distilled water and additional electrolyte preceded actual placement into the cell. Prevailing conditions, temperature 77° F and hydrogen pressure of 1-inch of water, were stabilized over a 20 to 30 minute period before a run. Oscilloscope pulses varied from 10 to 100-cycles per second, most being near 10 to 50-cycles per second. Decay rates of hydrogen from the silver surface were also measured. Four or five runs were made for each test piece, yielding desired data of current flow versus time and silver electrode potential versus time.

CHAPTER III

THEORY

Hydrogen Overpotential

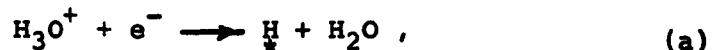
When an electrolytic solution contains metallic cations which are discharged as metal at the cathode, the electrode reaction in the case of irreversible electrodes is normally the discharge of hydrogen ions to form molecular hydrogen. With most metallic cathodes operating at small current densities, the potential becomes much more negative when current flows. The difference between the actual and the reversible electrode potential is the overpotential, given the symbol η . The overpotential is related to the current density I by the Tafel equation

$$\eta = a - b \log I, \quad 1$$

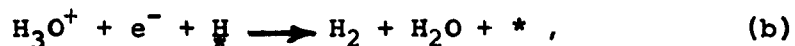
where a and b are constants. The current density is a measure of the rate of conversion of ions into molecular hydrogen, and the form of the Tafel equation suggests that some stage of this process takes place slowly and requires an activation energy (5). There has been much controversy over the nature of this rate-limiting step, and it is probable that it is not the same for all metals (7).

Several potentially slow steps have been considered:

(a) the passage, with desolvation, of protons from the solution to adsorption sites on the metal surface,



followed by either (b), an electrochemical reaction between a solvated proton, an adsorbed hydrogen atom, and an electron to yield hydrogen,



of (c), the combination of adsorbed hydrogen atoms,



It appears to be established that upon metals of a high overpotential, such as mercury and lead, the mechanism in aqueous acid solution consists of the slow discharge of protons onto adsorption sites on the cathode surface (a). On metals of very low overpotential, such as platinum, the rate-determining reaction appears to be the combination of hydrogen atoms (c), at least at low current densities. On metals of intermediate overpotential the strong adsorption of hydrogen atoms upon the metal surface, together with the fact that the value of b upon such metals is about 0.1, indicates the probability of the electrochemical mechanism (b).

If a metal electrode is placed in a solution with which it does not react, such as silver or platinum in dilute sulfuric acid, the initial potential of the metal-metal ion couple, as given by the Nernst equation

$$E = E^\circ - \frac{RT}{F} \ln M^+ , \quad 2$$

should be infinite since the concentration of the metal ion, M^+ , would be zero. There is an immediate local reaction, however, which may involve a reduction of hydrogen ions, an oxidation of the metal, or a reduction of some other species such as dissolved oxygen. Depending on the purity of the solution and the metal a more or less reproducible initial potential may be measured by means of a sensitive galvanometer or vacuum tube voltmeter that draws very little current. If, then, a small current is caused to flow through the system, a few microamperes per square centimeter, the potential rises to a new steady state value.

Bowden and Rideal (6) in their study of these phenomena found that the plot of potential versus time during the interval immediately following the start of current flow was nearly linear, as expressed by

$$-E = \Gamma/k + \text{constant} , \quad 3$$

where Γ represents the amount of active material on the surface. They found about 20×10^{-7} coulombs per square centimeter were required per 100 millivolts of overvoltage, regardless of the nature of the metal, so long as the rate of decay was small compared to the rate of build-up. The interpretation was that a layer of adsorbed hydrogen was developed and that there was a constant capacity for the double layer producing the overvoltage.

For mercury and amalgamated silver surfaces the value of k was about 0.6 microcoulomb per square centimeter of

apparent area per 100 millivolt change in overpotential. It was assumed in these cases the true surface area was equivalent to the apparent surface area. For other metals, notably platinum black, the greater charge required to produce the same overpotential was interpreted to mean that the effective area was greater than the apparent area. Since the system is studied in the absence of oxygen, the areas obtained are presumably those accessible to a layer of hydrogen atoms and are comparable to those measured by nitrogen gas adsorption.

The overpotential mentioned in the paragraphs above is known more specifically as activation overpotential. In addition to this phenomenon there may be concentration overpotential due to an ion gradient near the electrode surface and ohmic overpotential, arising either from current lines passing from the cathode to the anode or from the presence of a film (e.g. an oxide film) on the electrode surface which causes an appreciable resistance to the passage of current. These three kinds of overpotential may be distinguished by the manner in which they decay after cessation of the polarizing current: activation overpotential decays exponentially; concentration overpotential decays slowly and in a complex fashion; and ohmic overpotential decays instantaneously.

Dislocation and Plastic Deformation

Essentially the theory of dislocations is one of lattice defects, but it differs from previous theories in that

such defects are mobile, are susceptible to mathematical treatment with certain assumptions, and have quantitative significance in certain experimental studies.

An edge dislocation is formed in a crystalline solid when either a row of atoms is removed from a lattice or a row of atoms is displaced at unit distance. The dislocations can have different signs depending on whether a row of atoms is missing above the dislocation center (+) or below it (-). A positive and negative dislocation meeting on the same plane annihilate one another and perfect the lattice in that region. While the dislocation is centered about a line, its effect extends out into the surrounding lattice.

In the edge dislocation the motion that forms the dislocation (slip vector) is normal to the line of the dislocation. A screw or Burgers dislocation results when the displacement is parallel to the line of the dislocation. In addition there are partial, or Shockley dislocations, "sessile" dislocations, and variations of the different types.

Dislocations usually are present in metal crystals, for dislocation structure is precisely what is needed theoretically to perpetuate growth during lattice formation. Additional dislocations are introduced by plastic deformation. Such deformation in a crystal occurs by the movement of lamellae of the crystal over one another, as seen in Figure 7. Cahn (9) has shown how plastic bending in a crystal increases the number of edge dislocations.

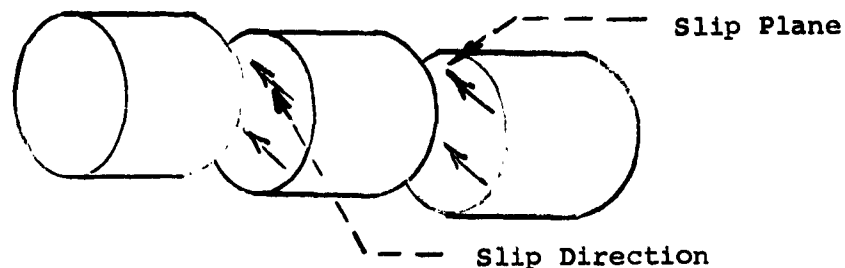


Figure 7- Sketch of movement on crystallographic slip planes in a crystal (3).

The displacement occurs along a crystallographic plane, the slip or glide plane, and in a crystallographic direction, the slip direction. In face centered cubic metals at normal temperatures, e.g. silver, the slip plane is usually the plane in the lattice that is most densely packed with atoms, (111), and the slip direction the one of greatest atomic density $[\bar{1}10]$.

There is a rather clearly defined stress, the critical resolved shear stress, at which a given crystal will begin to flow at an appreciable rate. Below this stress the rate of strain is so slow it requires long-time tests to measure it. The critical shear stress decreases with an increase in temperature, increases with impurity content, increases with prior deformation.

The strain energy of a dislocation is derived from the model introduced by Volterra (13), and the mathematical development of the energy relation may be followed in any of several texts (13, 20).

The strain energy per unit length of a screw dislocation is given by

$$E_s = \frac{Gb^2}{4\pi} \ln \frac{R}{r_0} \quad 4$$

where G is the shear modulus, b the Burgers vector of the dislocation, R the radius of influence of the dislocation in the surrounding lattice, and r_0 the radius of the core of the dislocation. For the edge dislocation the strain energy per unit length is given by

$$E_e = \frac{G b^2}{4\pi(1-\nu)} \ln \frac{R}{r_0} \quad 5$$

where ν is the Poisson ratio. In the above equations R should be comparable to the dislocation spacing in the lattice, and r_0 of a magnitude similar to the Burgers vector b . The maximum energy stored in lattice distortions as a consequence of plastic deformation has been measured thermally for several metals (20). Where the deformation is not too great, about 10 per cent of the energy expended in plastic flow is stored in the lattice. Upon continued plastic flow, however, the stored energy approaches a saturation value.

The density of dislocations is specified by giving the number of dislocation lines that intersect a unit area in the crystal. A one-to-one correspondence for dislocations and etch pits has been established through the grain-boundary experiments of Vogel. The X-ray line breadth broadening of plastically deformed metals also has yielded information

confirming the correspondence. Hendrickson and Machlin (17) have verified a thermal etching technique for revealing dislocations in silver, pertinent to this study. Winterbottom, et al (28) have extended the theory of thermal pitting to silver, suggesting the mechanism to be: impurity adsorption at dislocations, diffusion to the surface along dislocation pipes, and reaction with a surface impurity. The experimental work indicated that the critical conditions for microscopic thermal pit formation were low undersaturation of metal vapor and the presence of an impurity.

Chemical Reaction Rates

From statistical mechanics principles Eyring and coworkers (18) have developed the theory of absolute reaction rates. The essential feature of the theory is the postulation of an activated complex, an intermediate, unstable substance formed from the reactants and decomposing into the products. More development is apparently required before accurate numerical values can be determined for most reactions. From an engineering viewpoint experimental kinetic studies must still be made to determine reaction rates.

The general expression for the rate of reaction in a batch system is given quantitatively by the mass or moles of a product produced, or reactant consumed, per unit time per unit volume of reaction mixture,

$$r = \frac{dN}{Vd\theta} .$$

It is convenient to write the rate expression in terms of the limiting reactant H, and for a catalyzed batch reaction, the proper rate term would be

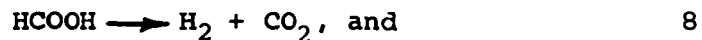
$$r = \frac{dN_H}{Wd\theta} , \quad 7$$

where W is the mass of catalyst used. Both direct evidence and theoretical deductions show that the rate may be a function of the activities of one or more of the components involved in the reaction. Often however the rate equation is simply a satisfactory relation which represents the data, since theoretical relations depend upon an exact knowledge of reaction mechanism and assumptions which are not strictly rigorous. Yang and Hougen (29) have discussed the determination of mechanisms of catalyzed gas reactions and surveyed the general procedures necessary in correlating experimental data.

The course followed by molecules in the main fluid phase which undergo catalysis are (a) mass transfer of reactants to the surface of the catalyst, (b) diffusional and flow transfer into the pore structure of the catalyst particle, (c) activated adsorption of reactants and activated desorption of products at the catalytic interface, (d) the surface reaction of adsorbed reactants to form chemically adsorbed products, (e) diffusional flow of products out of the pore structure, and (f) mass transfer of products from the surface to the main fluid phase. The resistances offered

by steps (a), (b), (e), and (f) are primarily physical in nature and for any but extremely fast reactions or extremely large porous catalyst particles may be minimized by using high mass flow rates. Concentration and temperature gradients are thereby largely eliminated, and some chemical aspect of the catalysis will likely be the rate-controlling step.

The decomposition of formic acid occurs according to two reactions:



However the extent of reaction 9 as promoted by silver or glass has been reported as negligible (22, 24). Reaction 8 has been reported as being zero order (22) and first order (24) when catalyzed by silver. Conditions for the zero order reaction were 50 to 70 millimeters of mercury formic acid pressure and reaction temperatures between 155 and 200° C. The first order reaction was observed at 160° and over a pressure range of 2.5 to 15 millimeters of mercury.

CHAPTER IV

RESULTS

Agreement between the experimentally measured dislocation density on the surface of a bent crystal and that calculated from theoretical considerations is noted in Figure 8. Specimen densities determined prior to the silver's use as a catalyst likewise compare well with those measured afterward, the measurements falling well within the limits of one standard deviation (see Table 5). For an unstrained surface the observed density was near that value found by others (17, 28).

Representative of the type of etch pits observed on some surfaces are those seen in Figure 9. Another type of pit, sharper and better defined than those in Figure 9, was produced on other surfaces. Similar differences in microscopic etch pits were noted (28) under varying conditions of black flux of silver, i.e. low silver undersaturation, and impurity concentration.

Hydrogen overpotential area data are shown in Figure 10 and Table 2, Appendix B. The curve of hydrogen overpotential area, hereafter abbreviated as HOA, versus dislocation density was fitted to the data by making the net area above the curve bounded by the experimental variation of the quantities measured equal to that below it. The systematic

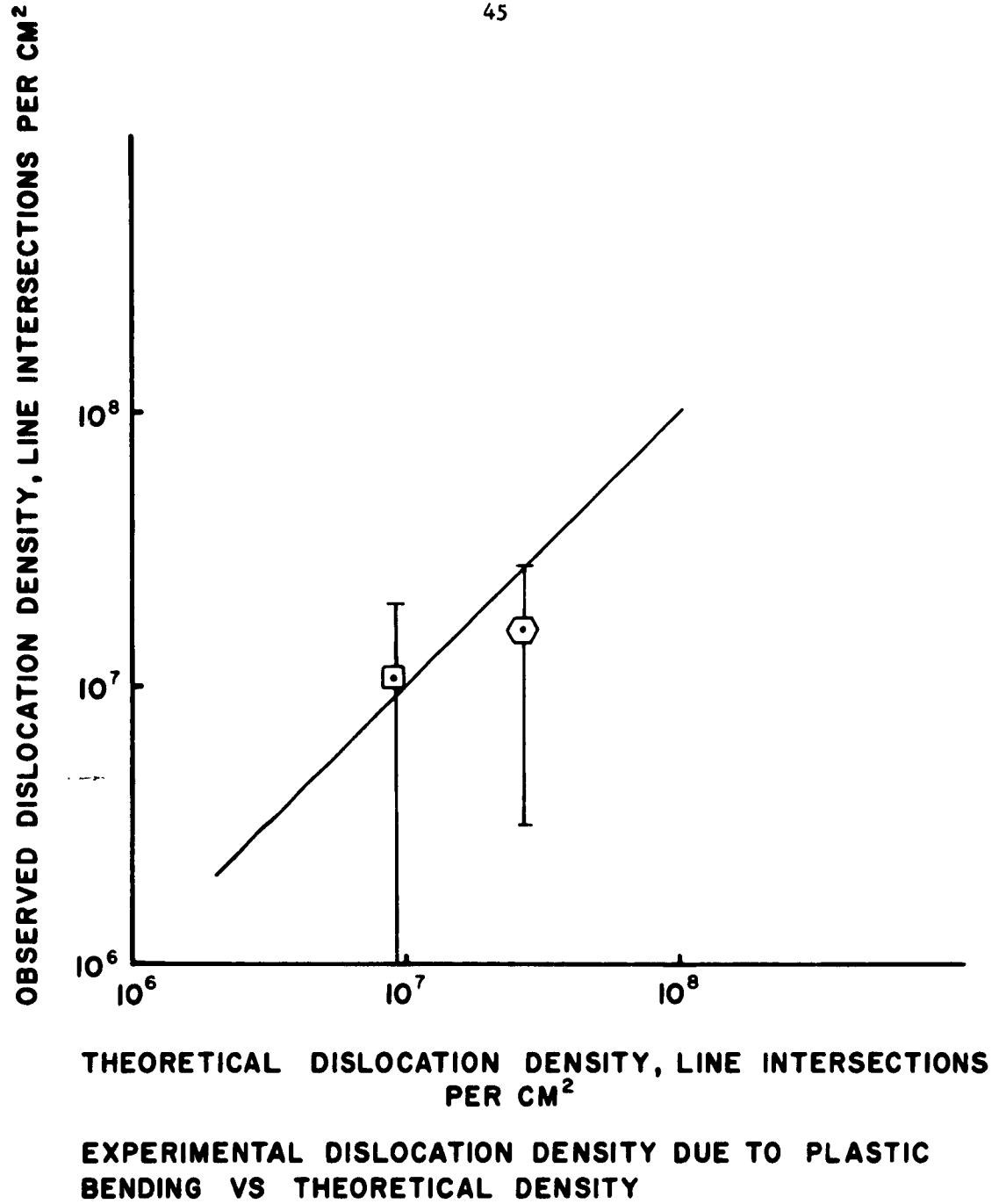


FIGURE 8

increase in HOA values with increasing dislocation densities suggests that surface preparation is not necessarily the controlling factor in the results. Sensitivity of the method to a macroscopic change in effective surface area was indicated by the result for a specimen mechanically polished with 240C silicon carbide disc. In this case the hydrogen overpotential area was about twice that obtained for specimens



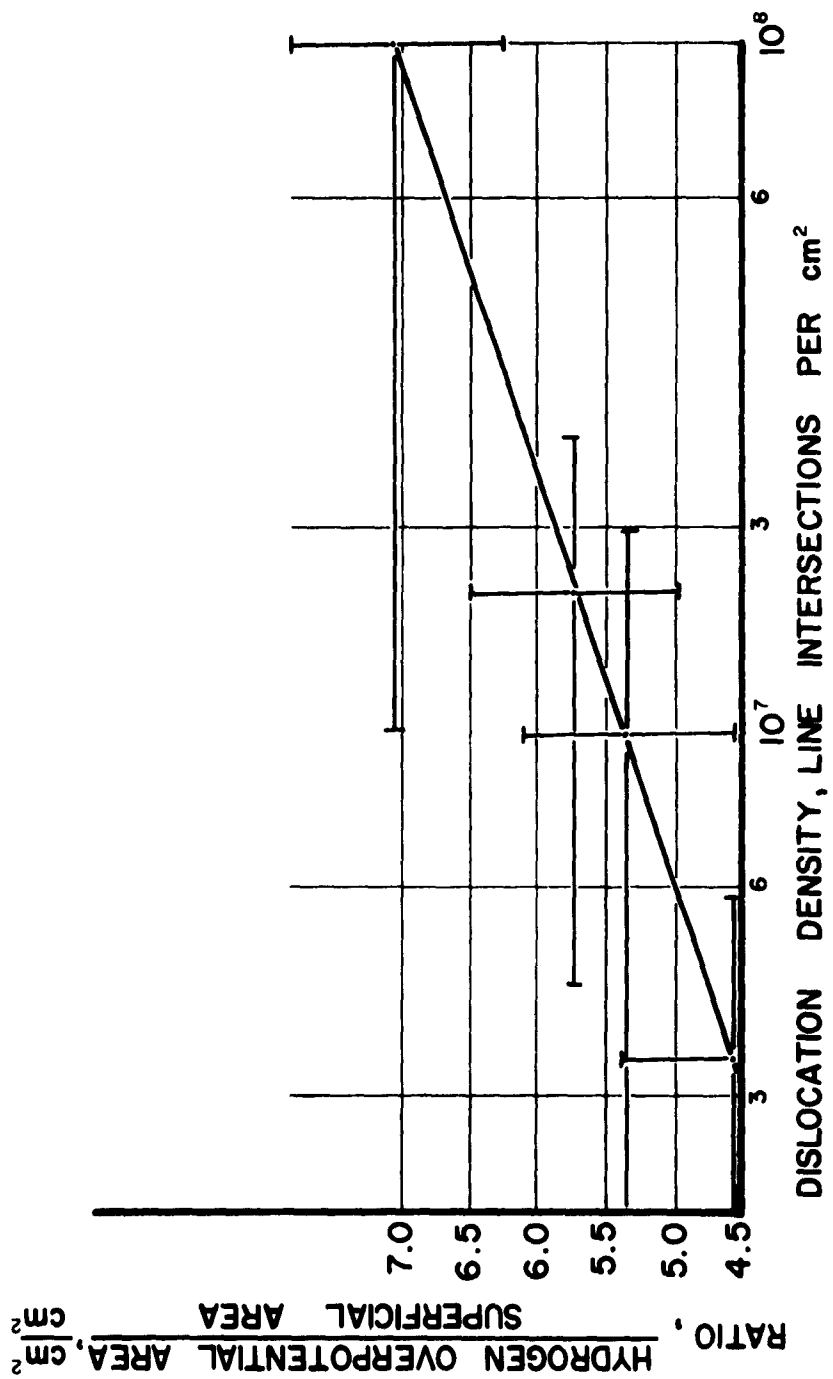
Figure 9- Etch pits on unstrained silver surface.
X2500 before publication.

prepared in the usual manner, i.e. mechanical polishing followed by electropolishing. Comparison of the HOA values for samples subjected to a pre-electrolysis and those not subjected to this treatment reveals a small variation which may be due to film formation. Further examination shows that the hydrogen overpotential area of the silver specimens was not appreciably affected by use of the material as a catalyst in the test reaction.

Formic acid decomposition rate curves are shown in Appendix B (Figures 15-26) for each of the measurements. The curves were obtained by drawing a smoothed curve through the product quantities measured and graphically differentiating the smoothed values to obtain a differential rate curve. The area under this curve was then determined, and if this value did not check the experimentally measured value of decomposition, another smoothed rate curve was drawn and the integration repeated until agreement was reached.

Initial rates, those extrapolated to zero time, covered a wide range of values. This variation is attributed to poorer precision in the analyses at the lower concentrations, rather than to any differences in film formation on the surfaces or reaction conditions. The same degree of precision in analysis was obtained over the entire range of concentrations, (See Figures 27 and 28, Appendix E); however as the concentration of products increased during the course of the reaction, the relative precision of their measurement increased. The significant portion of the rate curves was the final part, where the rate tended to approach a steady state value. Analysis was, in general, more precise in this region, and the weight of several analyses was reflected in the curve.

Since glass catalyzes the decomposition to yield the same products as does silver, it was necessary to evaluate the magnitude of this factor in the particular reaction system employed. This was done by exposing identically the same reaction system, amounts of fiberglas tape and other elements, e.g., vacuum grease, to formic acid vapor and measuring the extent of the reaction. The data given in Appendix D, Figures



Data points represent average of 13 to 20 measurements.
 VARIATION IN THE RATIO OF HYDROGEN OVERPOTENTIAL AREA
 (HOA) TO SUPERFICIAL AREA AS A FUNCTION OF DISLOCATION
 DENSITY.

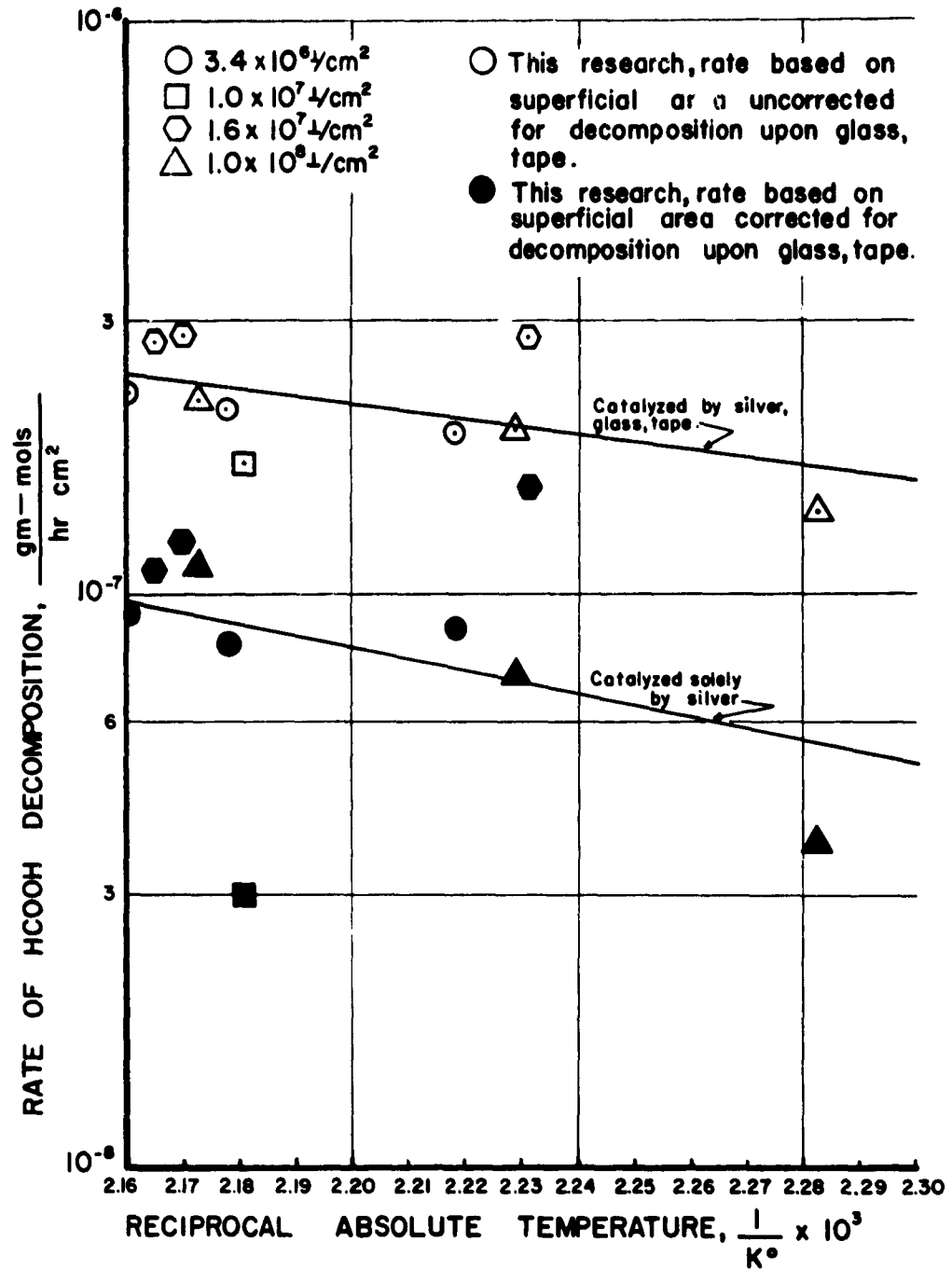
FIGURE 10

25 and 26, are somewhat higher than those reported elsewhere (22), although within the range of experimental precision. Figure 32 illustrates the influence of temperature on these measurements.

Differences in partial pressure and temperature, existing between material in the bulk of the vapor and at the interface of the catalytic surface were calculated by the method of Yang and Hougen and were negligible, i.e. less than 0.001-millimeter mercury and 0.01° F, respectively. In general partial pressure film gradients become negligible where surface reactions proceed slowly and where high partial pressures of the reactants are encountered, both conditions applicable to this research. Also temperature gradients tend to be minimized where the surface reaction is slow.

Over the range of experimental temperatures and pressures employed, the decomposition of formic acid behaved as a zero order reaction and yielded carbon dioxide and hydrogen as products. The negligible effect of pressure upon the decomposition rate is shown by Figure 30, Appendix F. If the reaction were zero order with respect to formic acid, then a plot of the acid partial pressure with time should be linear. Such a plot is demonstrated by Figure 31 of Appendix F. It was therefore concluded that the reaction rate was essentially independent of pressure. Although no particular attempt was made to analyze the reaction mechanism, pressure and temperature effects had to be evaluated to isolate the influence of dislocation density upon the rate.

Figure 11 is an Arrhenius plot of the decomposition rate versus the reciprocal absolute temperature. Both curves



TEMPERATURE DEPENDENCE OF CATALYZED DECOMPOSITION RATE OF FORMIC ACID, BASED ON SUPERFICIAL AREA.

FIGURE II

were fitted to the data by the method of least squares. The upper curve represents the gross rate of decomposition per square centimeter of silver superficial area as catalyzed by both silver and glass, while the lower curve is the rate as promoted solely by the silver. Except for two points the data are within a range of 3.0×10^{-8} gram-moles per hour per square centimeter of the lower curve. However these two points lie within the limits of the probable mean error of the measurements (see Appendix G for summary of errors).

Thus far no consideration has been given to the variation in the dislocation density in deriving the rates of decomposition. It is reasonable to assume that this factor can be included in the area term which appears in the rate expression. According to reaction kinetics theory, the superficial area should have little, if any, theoretical significance. The so-called true or active area for reaction is usually obtained by measuring the amount of gas absorbed on the surface as in the well-known BET technique. To obtain reliable values by this method, surface areas of the order of square meters per gram are needed. Since the superficial surface area of the crystalline silver in this research was only in the neighborhood of 0.3 square centimeters per gram and since the quantity of pure single crystal silver was limited, it was necessary to resort to another technique for evaluating an "active" area, namely the hydrogen overpotential area as discussed in Chapter III.

The value of the hydrogen overpotential area (hereafter abbreviated, HOA) is dependent on the constant, k_{HOA} ,

used in the following equation:

$$k_{\text{HOA}} = \frac{\Gamma/\text{cm}^2}{\Delta E} \quad 10$$

where,

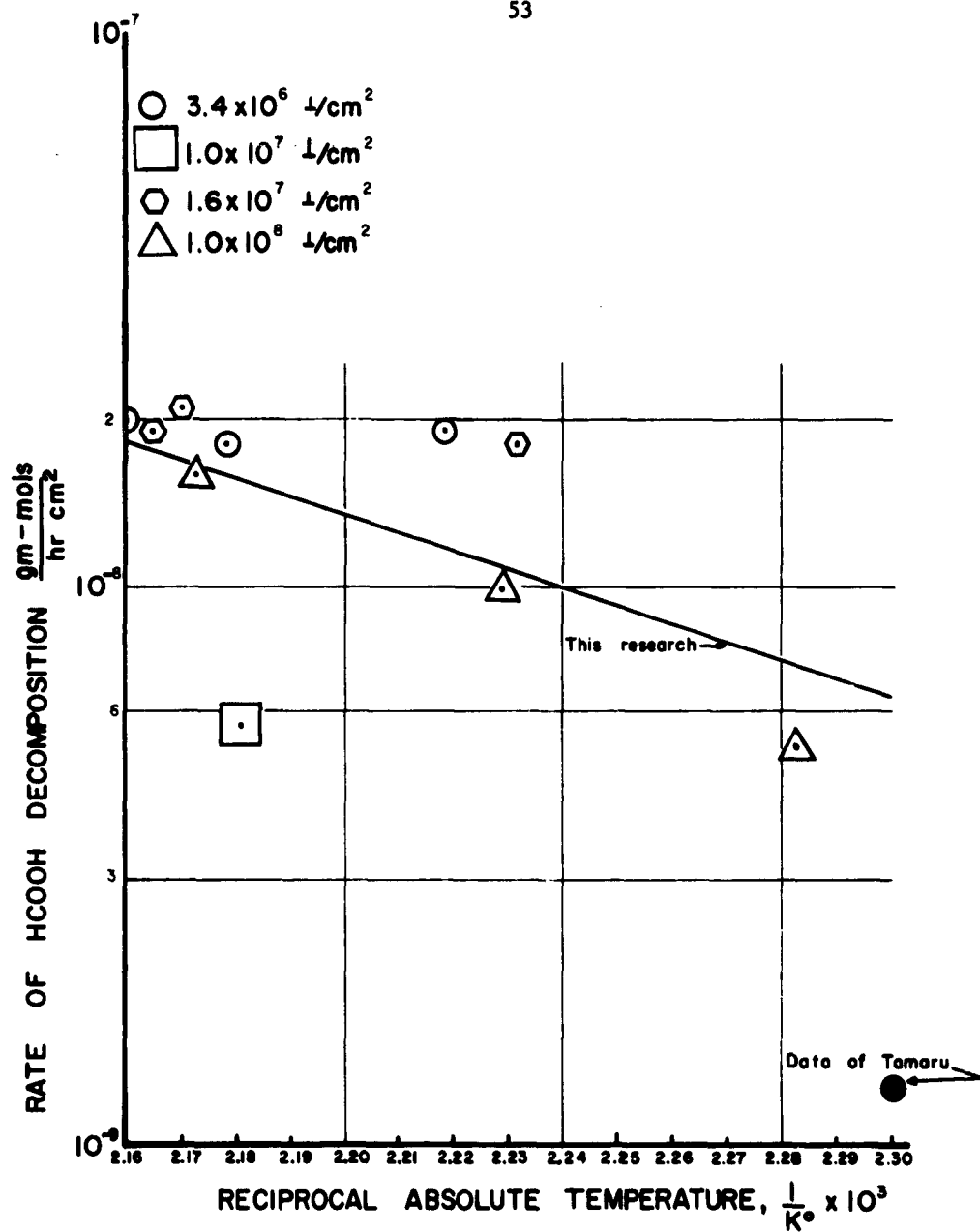
Γ = quantity of electricity passed, coulombs

E = voltage of the metal electrode undergoing polarization, volts

$k_{\text{HOA}} = \mu\text{f}/\text{cm}^2$ (taken as 12 in this research).

There is some disagreement in the literature (2) regarding the correct value for the constant to be used in Equation 10, values ranging from 5 to 20. A value of 12 was selected arbitrarily as a representative mean in this research for calculating the HOA, from which the Arrhenius plot in Figure 12 was obtained. It is to be noted that the rate value reported by Tamaru (24) at 160°, which is based on a BET area, is about one-fifth that observed in this research based on HOA area. This discrepancy could have been reconciled had the value for the constant in Equation 10 been taken as 2.4 rather than 12. In fact, Bowden and Rideal (6) originally reported a value of 6 but later retracted it on the basis of impurities in their mercury. Furthermore, the apparent difference in the BET and HOA area is not unexpected since the former is a measure of the physical or van der Waals absorption whereas the latter is a chemisorption area. Typical values for HOA obtained in this research are given in Table 2, Appendix C.

The uncertainty in the constant was circumvented in the following manner. The ratio of the HOA for the (211)

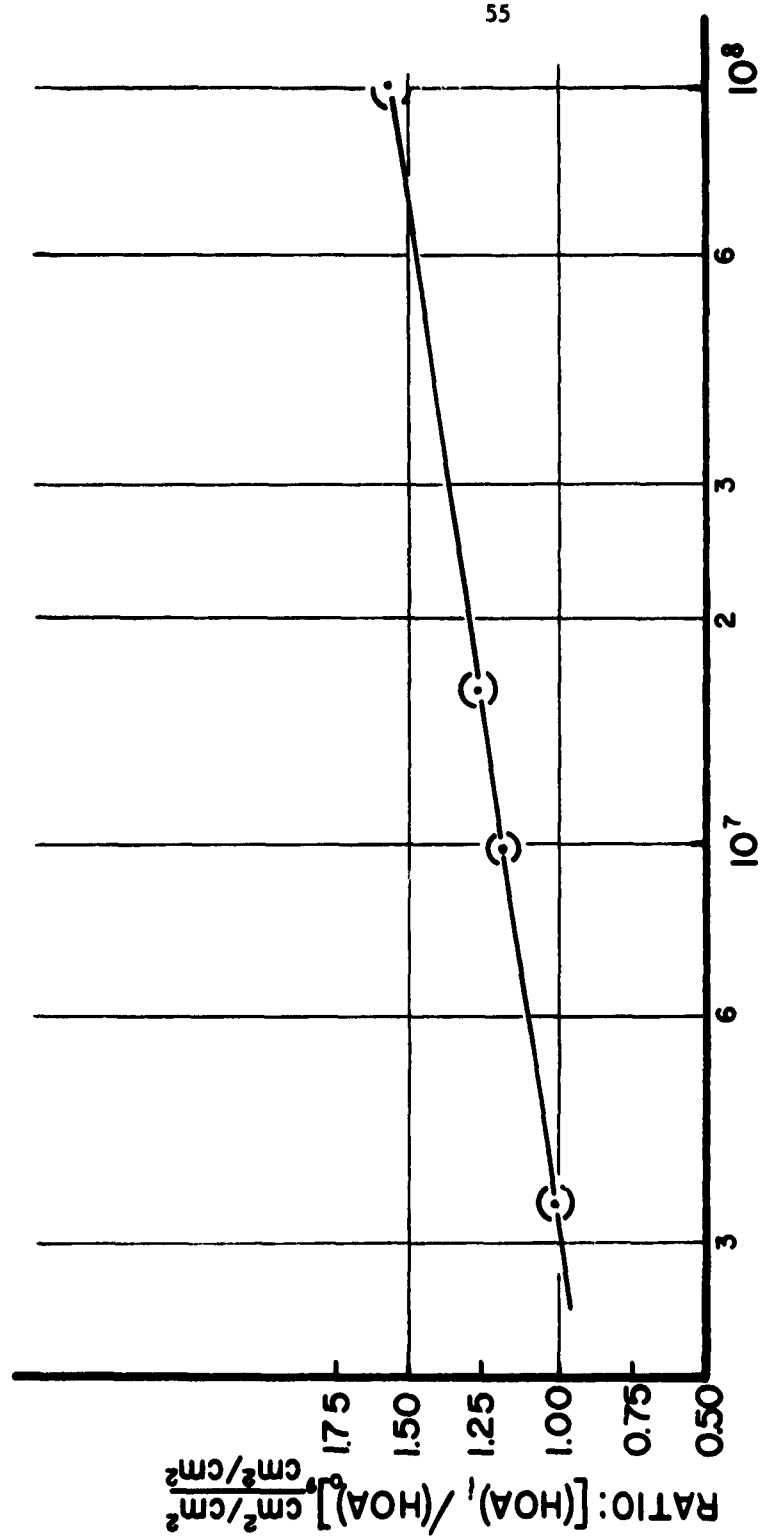


TEMPERATURE DEPENDENCE OF CATALYZED DECOMPOSITION RATE OF FORMIC ACID, BASED ON HYDROGEN OVERPOTENTIAL AREA.

FIGURE 12

surface with $\bar{\rho}$ dislocations, $(HOA)_1$, to that for the as grown (211) surface with 3.2×10^6 dislocations per square centimeter, $(HOA)_0$, was computed from an average of 13 to 20 measurements for each data point and was plotted against the dislocation density. This ratio is independent of the constant used to compute the HOA values. The results are shown in Figure 13.

When this dimensionless factor, $(HOA)_1/(HOA)_0$, is multiplied by the superficial surface area, the result obtained represents an hypothetical, active area corrected for the variation in dislocation density. Therefore the rate curve shown in the lower part of Figure 11 can be corrected by this ratio to obtain the line (determined by the method of least squares) shown in Figure 14. The data agree within experimental error with that of Sosnovsky (22), who based his rates on the superficial area of the (100) and (111) planes of crystals as grown without any surface preparation. Although he did not report the dislocation density, the value is estimated to be $3.0 \times 10^6 \text{ } \bar{\rho}/\text{cm}^2$ based on this present work, which is in good agreement with values reported by two other investigators (17, 28). In view of the correspondence of the rate data obtained herein with that of Sosnovsky, this method proposed for correcting the superficial area is significant. The activation energy is calculated as 15.0 kilocalories per gram mole. This value is less than the activation energy obtained by Sosnovsky for the lower order (100) and (111) planes.

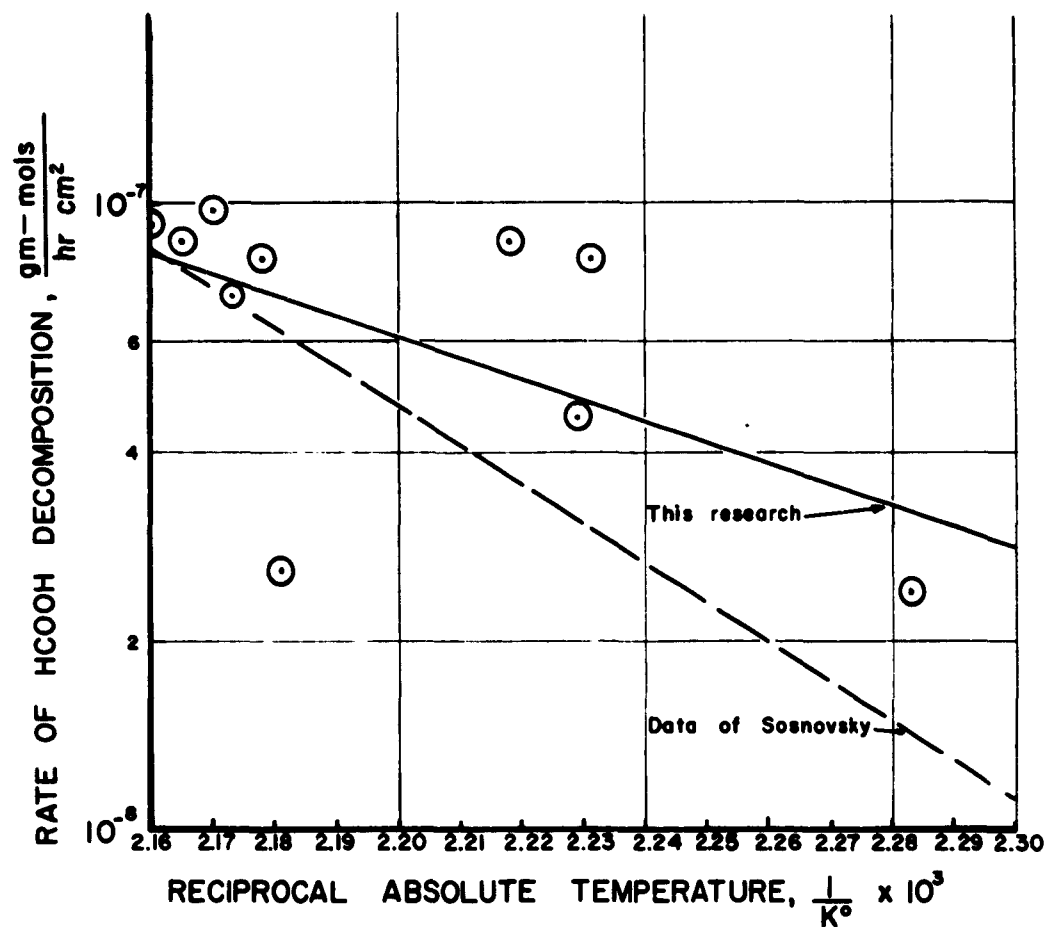


DISLOCATION DENSITY, LINE INTERSECTIONS PER cm²

[HVA]₀ = 4.57 cm² at 3.4 × 10⁶ L/cm²

VARIATION OF THE HOA RATIO WITH DISLOCATION DENSITY.

FIGURE 13



TEMPERATURE DEPENDENCE OF CATALYZED DECOMPOSITION RATE OF FORMIC ACID, BASED ON HYPOTHETICAL ACTIVE AREA.

FIGURE 14

Discussion of Results

Reaction rates were measured under conditions such that mass transfer effects should not have been rate-controlling, and the values obtained correspond with those of other investigators. Interpretation of the data indicated that the reaction mechanism did not change, and apparently the presence of decomposition products and air did not poison the catalyst appreciably. Neither was there a change in the dislocation density or hydrogen overpotential area of the catalyst as measured before and after the reaction.

It was hoped that the catalytic activity of silver could be related either to the theoretically calculated dislocation energy or to the energy expended in cold working the metal, computed values for which are shown in Appendix I. However both the theoretical energy attributed to the dislocations present and the energy of cold work are several orders of magnitude smaller than any energy term which would interpret the variation in rates. Furthermore the correlating factor for dislocation density appears to be independent of temperature over the limited range of reaction temperatures investigated, a fact which argues against any strong dependence on energy considerations. Although it is probable that resoftening and recrystallization processes operated to some degree to relieve the lattice distortions caused by the cold work, significant is the fact that the dislocation arrays with higher energy levels in the grain boundaries of specimen 422A

did not produce any great variation in rate. For these reasons it is unlikely that energetics are responsible for the observed results.

The data show that the relative catalytic activity of the (211) plane of silver can be altered by varying its dislocation density, the alteration amounting to a factor of about one and one-half with a hundredfold variation in dislocation density. This variation is related to the change in active area as measured by the hydrogen overpotential technique. It is not correct to assume that this area is in the strictest sense a geometric area, for analysis shows it is unlikely that the increased dislocation line intersections actually would increase the geometric area to the extent reflected in the HOA measurements.

Rather unexpected is the fact that the polycrystalline specimen failed to show a disproportionately high relative HOA value as compared to that of the single crystal specimens. The dislocation density value within average single grain of the recrystallized specimen was about 10^8 line intersections per square centimeter; however the grain boundaries contributed an undetermined number of dislocations to the total dislocation population. It would appear that the HOA ratio might be reaching a limiting value near this dislocation density.

CHAPTER V

CONCLUSIONS

1. Excess dislocation densities above 10^6 intersections per square centimeter increase the area of a metal as determined by the hydrogen overpotential technique. The increase is approximately fifty percent for a hundred-fold increase in dislocation density.
2. Dislocations in a silver catalyst have a small effect on the relative catalytic activity of the metal; the effect is associated with the hydrogen overpotential area.

REFERENCES

1. Abrahams, M. S., Sc.D. Thesis, Columbia University (1958).
2. Adamson, A. W., Physical Chemistry of Surfaces, New York: Interscience Publishers, Inc. (1960), p. 443.
3. Barrett, C. S., Structure of Metals, New York: McGraw-Hill Book Co., Inc. (1952), p. 336.
4. Bicelli, L. P. and Rivolta, B., "Researches on Hydrogen Overvoltage on Metallic Single Crystals: Silver and Lead," WADC Technical Note 59-393 (April, 1960).
5. Bond, G. C., Catalysis by Metals, London and New York: Academic Press (1962), p. 177.
6. Bowden, F. P. and Rideal, E. K., Proceedings of the Royal Society (London), A120, 59 (1928).
7. Butler, J. A. V., Electrical Phenomena at Interfaces, London: Methuen and Co., Ltd. (1951).
8. Cabrera, N., in Semiconductor Surface Physics, R. H. Kingston, editor, Philadelphia: University of Pennsylvania Press (1957), p. 327.
9. Cahn, R. W., Journal of the Institute of Metals, 76, 613 (1950).
10. Chalmers, B., Canadian Journal of Physics, 31, 132 (1953).
11. Chalmers, B., Modern Research Techniques in Physical Metallurgy: American Society for Metals, Cleveland, Ohio (1953).
12. Coleman, R. V., and Laukonis, J. V., Journal of Applied Physics, 30, 1364 (1959).
13. Cottrell, A. H., Dislocations and Plastic Flow in Crystals, Oxford: At the Clarendon Press (1953), p. 31.
14. Cratty, L. E. and Granato, A. V., Journal of Chemical Physics, 26, 96 (1957).

15. Gwathmey, A. T. and Lawless, K. R., The Surface Chemistry of Metals and Semiconductors, New York: John Wiley & Sons, Inc. (1960), p. 495.
16. Hall, W. K. and Emmett, P. H., Journal of Physical Chemistry, 63, 1102 (1959).
17. Hendrickson, A. A. and Machlin, E. S., Acta Metallurgica, 3, 64 (1955).
18. Hougen, O. A. and Watson, K. M., Chemical Process Principles, Part III, New York: John Wiley & Sons, Inc. (1953).
19. Kehl, G. L., Principles of Metallographic Laboratory Practice, New York: McGraw-Hill Book Co., Inc. (1943).
20. Kittel, C., Introduction to Solid State Physics, New York: John Wiley & Sons, Inc. (1961), p. 545.
21. Sherwood, T. K. and Reed, C. E., Applied Mathematics in Chemical Engineering, New York: McGraw-Hill Book Co., Inc. (1939), p. 360.
22. Sosnovsky, H. M. C., Journal of Chemical Physics, 23, No. 8, 1486 (1955).
23. Sosnovsky, H. M. C., Journal of the Physics and Chemistry of Solids, 10, 304 (1959).
24. Tamaru, K., Transactions of the Faraday Society, 55, 824 (1959).
25. Tuul, J. and Farnsworth, H. E., Journal of the American Chemical Society, 83, 2247 (1961).
26. Wang, H. L. and Hackerman, N., Journal of Physical Chemistry, 56, 771 (1952).
27. Wilson, J. N., Voge, H. H., Stevenson, D. P., Smith, A. E., and Atkins, L. T., Journal of Physical Chemistry, 63, 463 (1959).
28. Winterbottom, W. L., Robinson, W. H. and Hirth, J. P., "Thermal Etch Pits and Dislocations in Silver," AFOSR Technical Note 731 (March, 1961).
29. Yang, K. H. and Hougen, O. A., Chemical Engineering Progress, 46, No. 3, 146 (1950).
30. Young, F. W., Journal of Applied Physics, 29, 760 (1958).

APPENDIX A
NOMENCLATURE

NOMENCLATURE

a_m	Surface area of pellets per unit mass
a_p	Surface area per single catalyst pellet
b	Burgers vector of dislocation
C_p	Specific heat at constant pressure
D_{A_m}	Mean diffusivity of component A in gas mixture
E	Potential
E°	Reversible potential
E_e	Energy of edge dislocation
E_s	Energy of screw dislocation
f	Farad
F	Constant
G	Mass velocity; shear modulus
HOA	Hydrogen overpotential area
ΔH	Heat of reaction
I	Current density
k	Thermal conductivity
k_{HOA}	Constant, 12 microfarads cm^{-2}
M_m	Mean molecular weight
N	Gram molecular weight
P	Pressure
P_f	Pressure factor, gas film
r	Rate of reaction
r_o	Radius of core of dislocation
R	Gas constant; radius of influence of dislocation in surrounding lattice
T	Absolute temperature

V Volume
W Mass

Greek Letters:

α Constant
 α^1 Constant
 Γ Quantity electrical charge, coulombs
 ϵ Strain
 ν The Poisson ratio
 μ Viscosity; probable mean error; micro-; micron
 ρ Density
 σ Standard deviation
 τ Shear stress
 Ω Ohms

APPENDIX B
DISLOCATION DENSITY DATA AND SAMPLE
DATA SHEET AND DENSITY CALCULATION

TABLE 1
DISLOCATION DENSITY DATA

Specimen	Bend Radius cm.	Number of Measure- ments	Before Reaction Line Inter- sections per cm ²	Number of Measure- ments	Following Reaction Line Inter- sections per cm ²	Average Line Inter- sections per cm ²	Calculated From Theory Line Inter- sections per cm ²
524B	---	7	0.35×10^7	8	0.29×10^7	0.32×10^7	---
411A	4.0	5	1.55×10^7	9	0.75×10^7	1.03×10^7	0.9×10^7
410A	1.32	11	1.59×10^7	8	1.55×10^7	1.57×10^7	2.7×10^7
422A	Cold rolled	5	10.00×10^7		---	10.00×10^7	---

Sample Data Sheet and Sample Calculation

Dislocation Density

Run 2410A

Lenses for metallograph: X12.5° and Fluor X85

Bellows setting: 424 mm.

Magnification: X2000

Sample Number	Etch Pits	Area Viewed On Metallograph Screen cm ²
1	120	4.0 x 7.35
2	189	3.5 x 9.7
3	111	9.7 x 3.1
4	145	9.7 x 3.7
5	240	9.7 x 7.35
6	150	4.0 x 7.35
7	143	9.7 x 7.35
8	229	9.7 x 7.35

Calculation Dislocation Density Sample No. 1

$$\frac{120 \text{ Etch Pits}}{4.0 \times 7.35 \text{ cm}^2 / 2000 \times 2000} = 1.63 \times 10^7 \text{ Line Intersections per cm}^2$$

APPENDIX C
HYDROGEN OVERPOTENTIAL DATA AND SAMPLE
DATA SHEET AND SAMPLE CALCULATION

TABLE 2

HYDROGEN OVERPOTENTIAL AREA DATA*

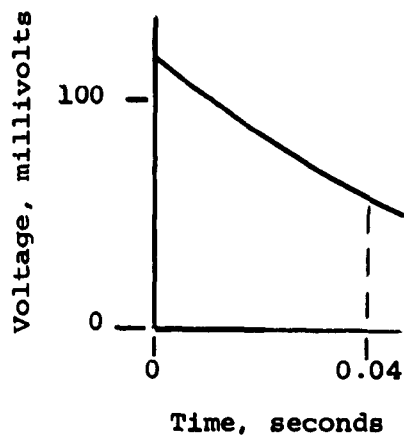
Specimen	Dislocation Density	$\frac{\Delta\Gamma/\text{cm}^2}{\Delta E}$	Before Reaction HOA	Following Reaction HOA
	Line Intersections per $\text{cm}^2 \times 10^{-7}$	$\frac{\mu\text{f}}{\text{cm}^2}$	cm^2/cm^2 S.A.	cm^2/cm^2 S.A.
524B	0.32	55.3	4.61	
524B	0.32	54.3		4.53
524B ₂	0.32	58.7		4.89
411A	1.00	66.7	5.56	
410A	1.57	67.2	5.60	
422A	10.00	83.2	6.93	
422A	10.00	83.7		6.97
E ₃		128.1	10.69	
K ₄	7.10	73.4	6.12	

*These data were obtained under the following conditions:

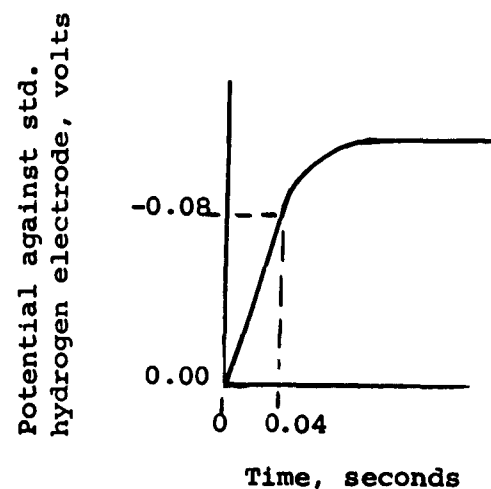
1. Mercury standard of $\frac{\Delta\Gamma/\text{cm}^2}{\Delta E} = 12 \mu\text{f}/\text{cm}^2$ employed to calculate HOA values.
2. Not subjected to pre-electrolysis before measurement.
3. Mechanically polished with 240C silicon carbide polishing disc.
4. Measurement made prior to dislocation density determination.

Hydrogen Overpotential Area Data

Mass: 0.875 grams
 Superficial surface area: 0.738 cm²
 Dislocation density: 1.00 x 10⁷ intersections/cm²



From Sanborn recorder chart



From oscilloscope picture

Sample Calculation

$$\frac{3.91 \text{ mv-sec}}{1000 \ \Omega} \frac{\text{volt}}{1000 \text{ mv}} = 3.91 \times 10^{-6} \text{ coulombs}$$

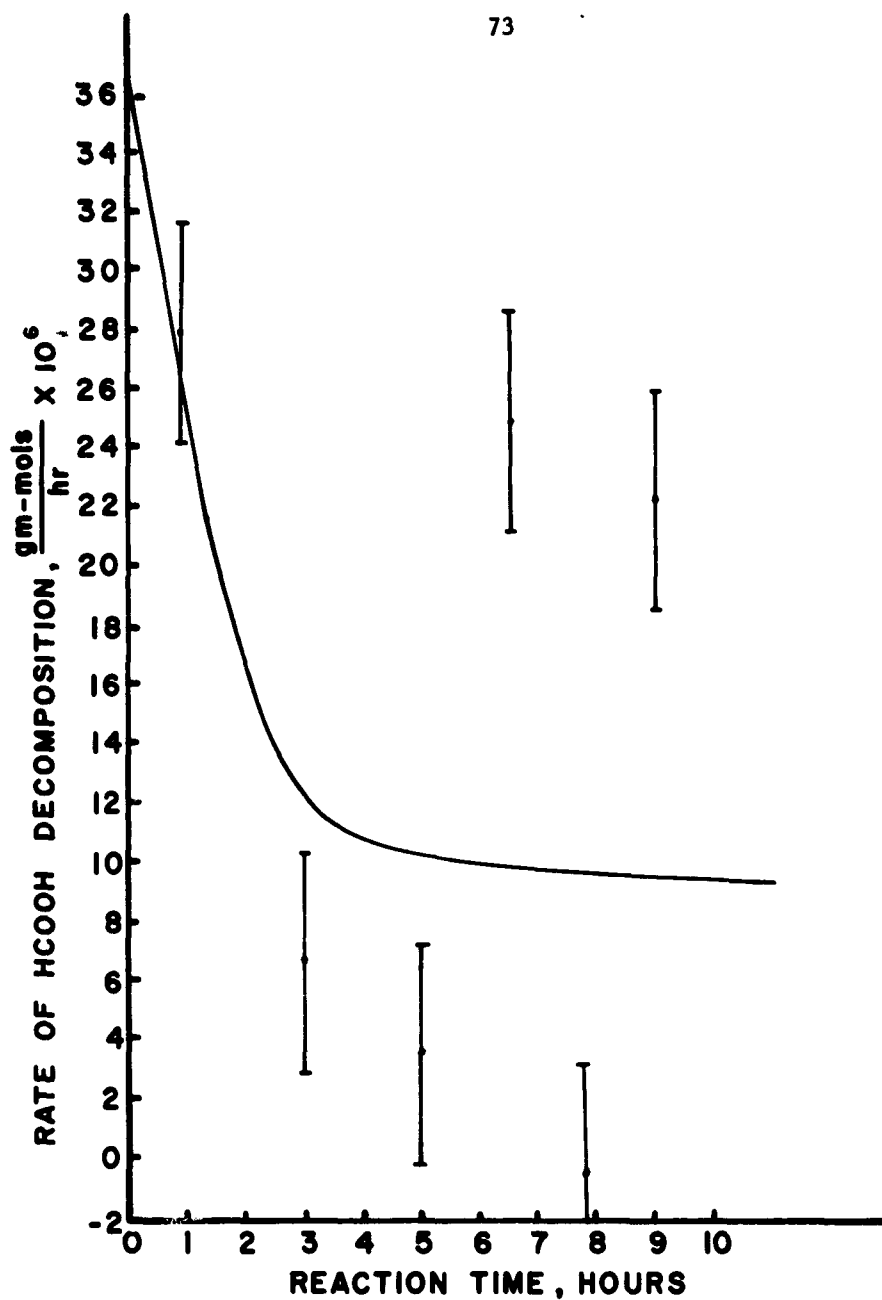
$$\frac{\Delta\Gamma/\text{cm}^2}{\Delta E} = \frac{3.91 \times 10^{-6} \text{ coulombs}/0.738 \text{ cm}^2}{0.08 \text{ volt}} =$$

$$66.3 \times 10^{-6} \frac{\text{coulombs}}{\text{volt cm}^2}$$

APPENDIX D
FORMIC ACID DECOMPOSITION RATE DATA AND SAMPLE
DATA SHEET AND RATE CALCULATION

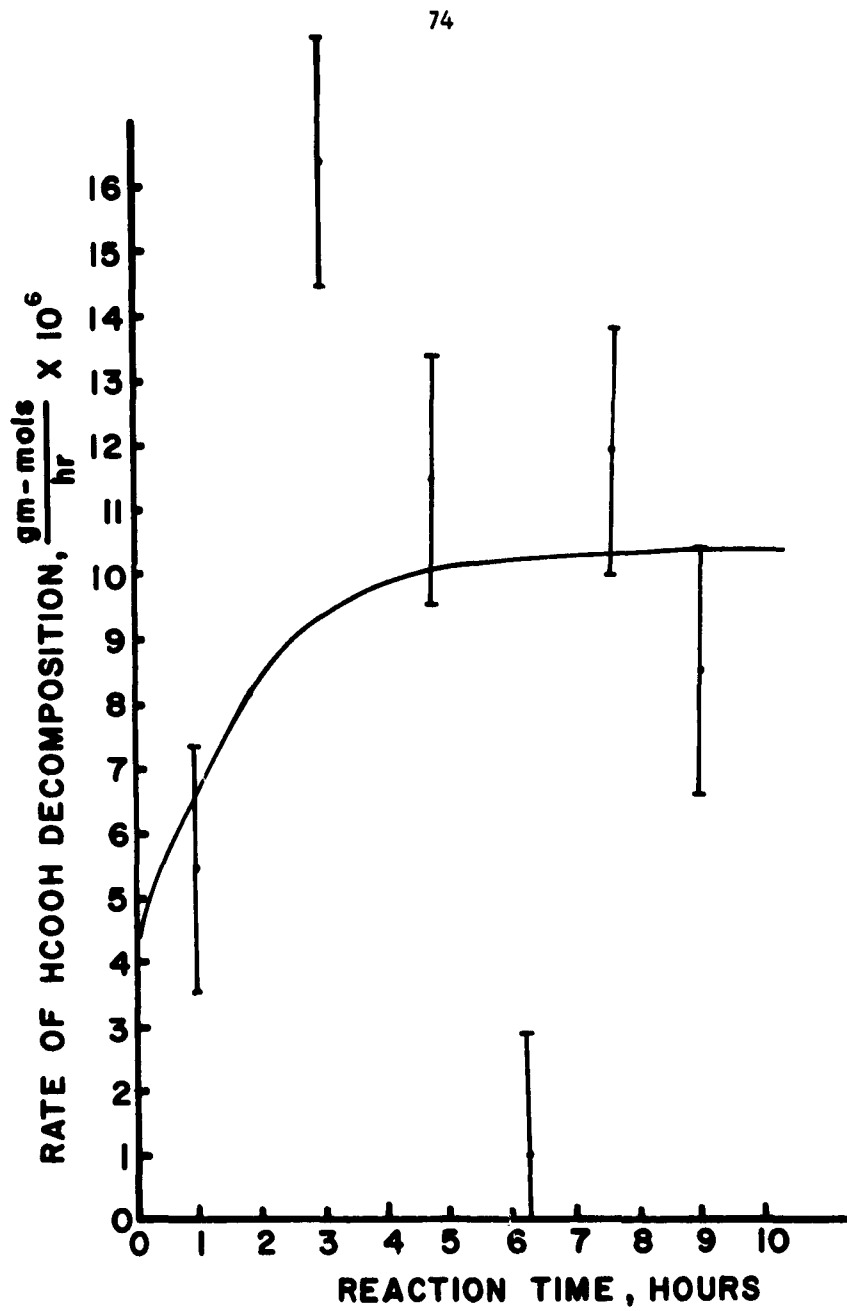
FORMIC ACID DECOMPOSITION RATE DATA

Figures 15 to 26 present the rate curves, which were derived from the concentration data. The concentrations were first smoothed and then graphically differenced to establish a trial rate curve. The area under this curve was then determined. If the result did not agree with the experimentally measured value, another trial rate curve was drawn and the process repeated until the calculated and measured values of decomposition agreed.



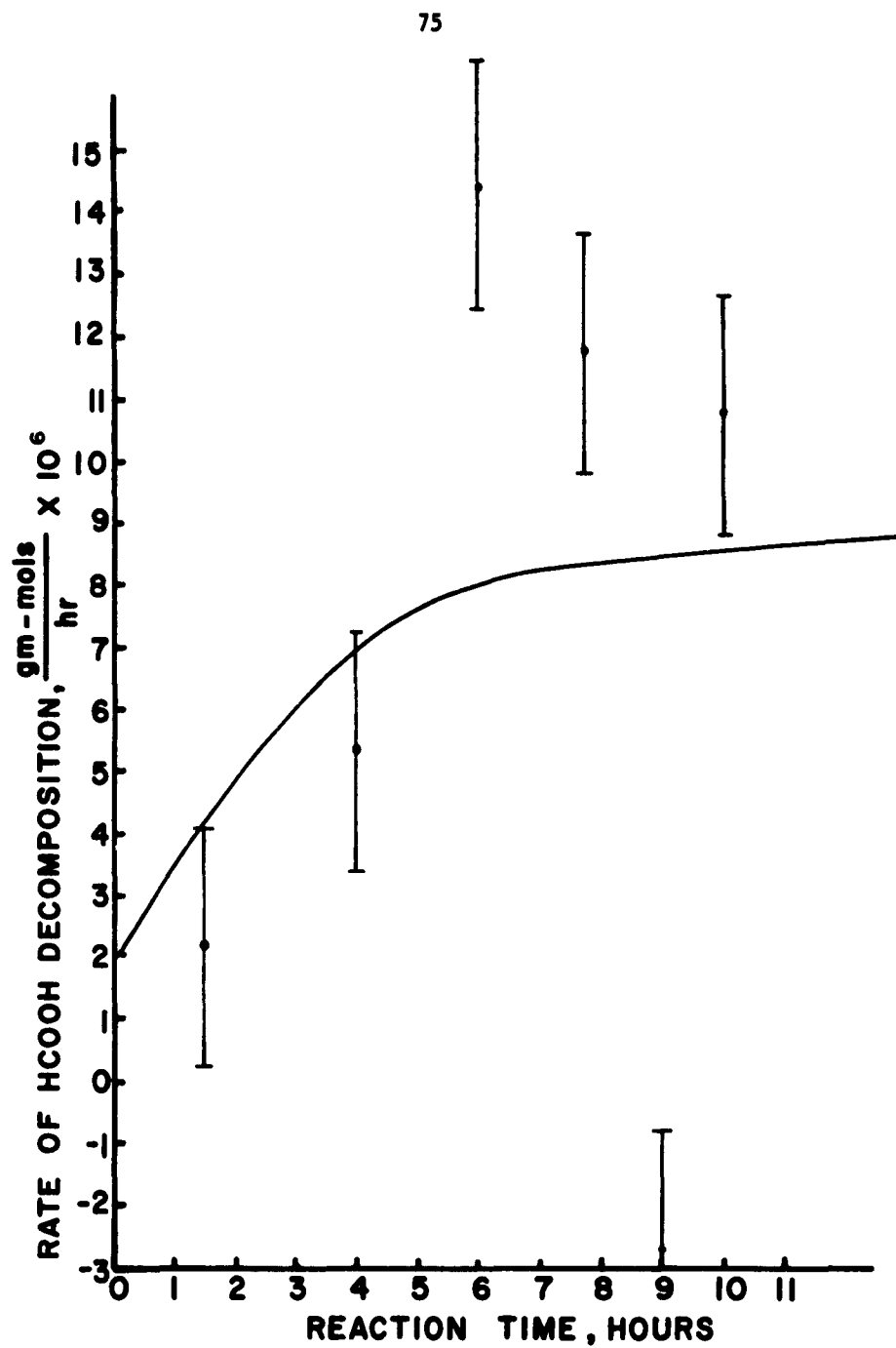
524 B
186.0 \pm 1.1 $^\circ$ C
46.13 cm 2
3.4 X 10 6 L/cm 2

FIGURE 15



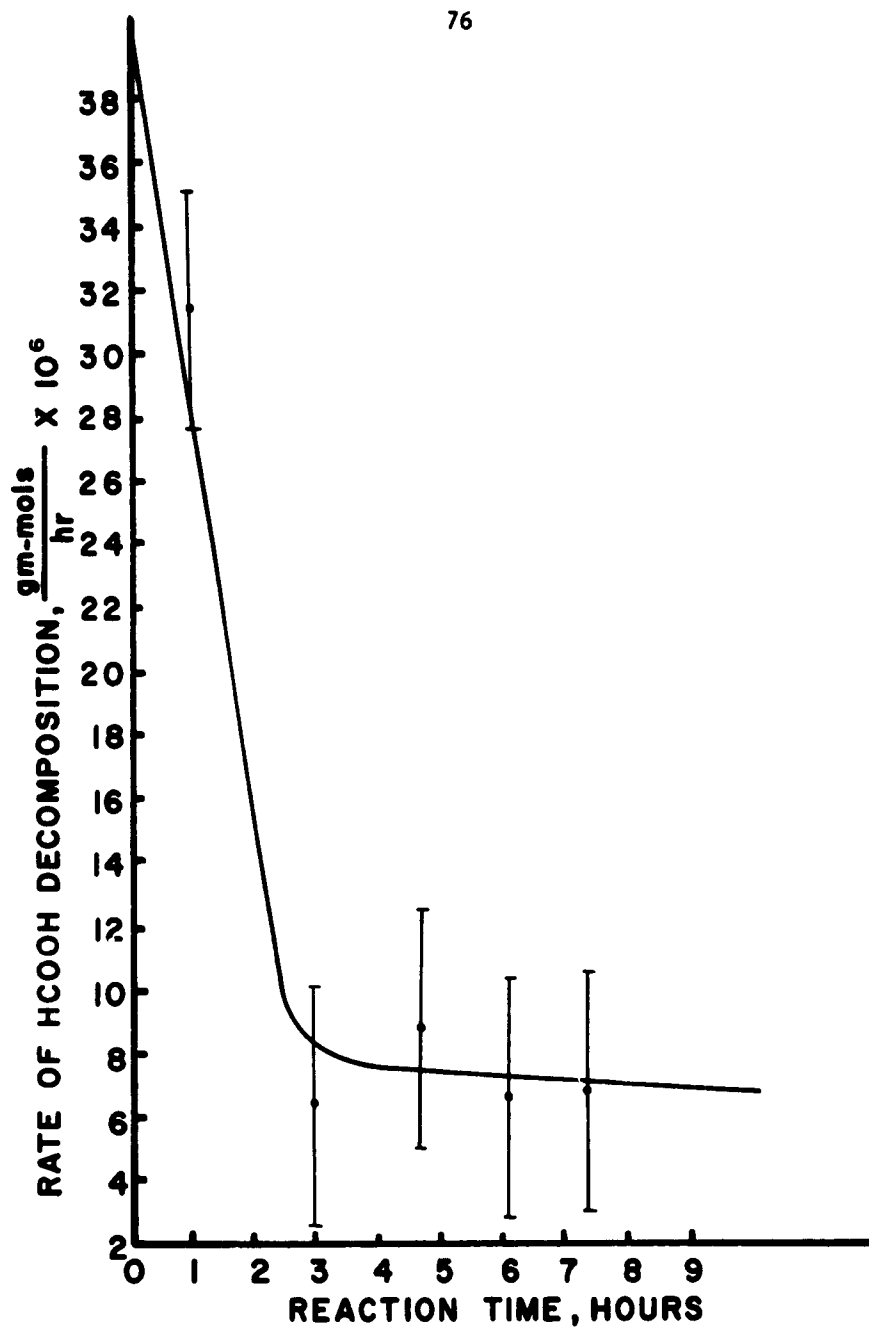
2524 B
 189.8° ± 1.1°C
 46.13 cm²
 3.4 × 10⁶ 1/cm²

FIGURE 16



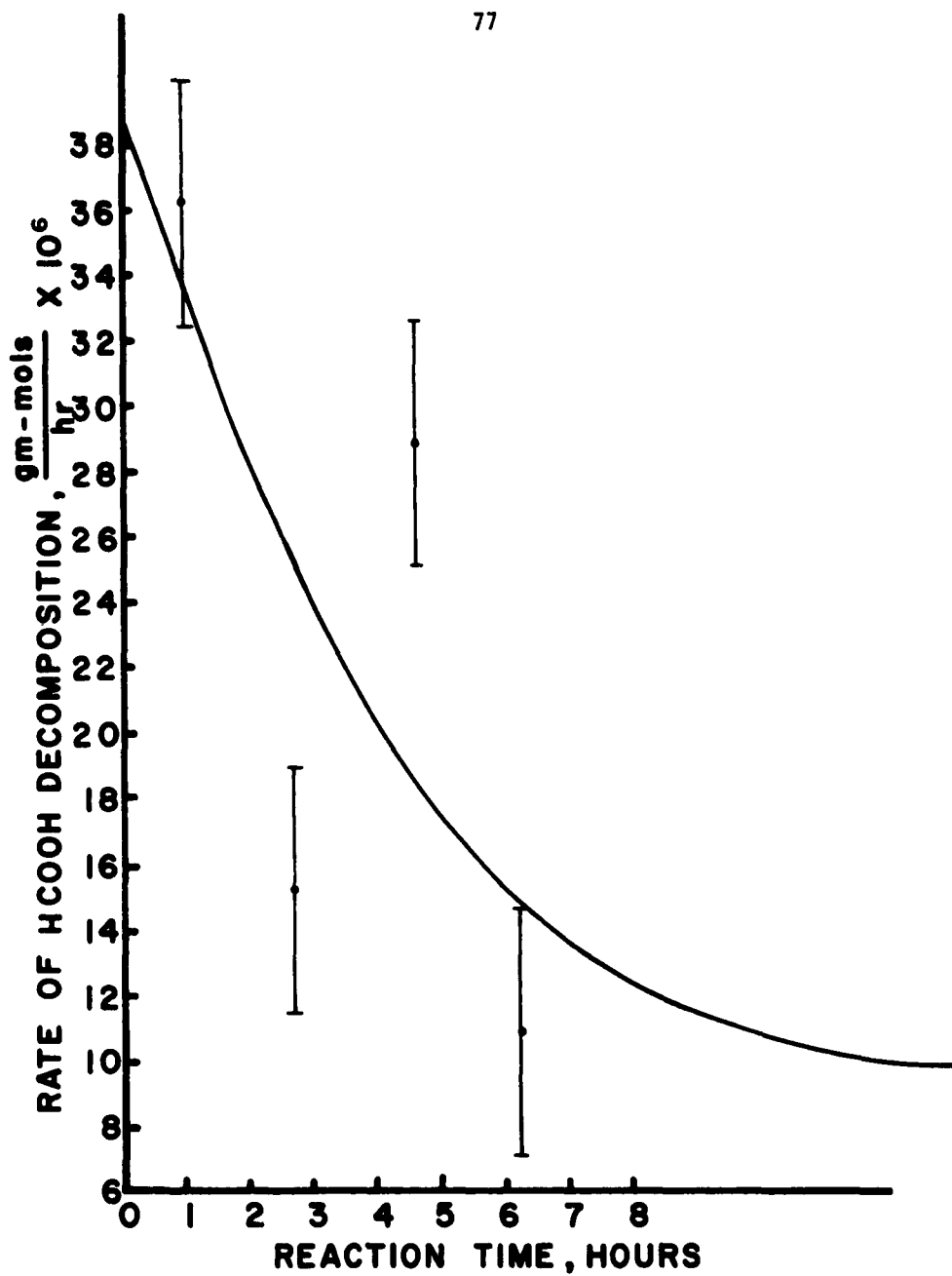
3524 B
177.8° ± 1.1°C
46.13 cm²
3.4 × 10⁶ μ /cm²

FIGURE 17



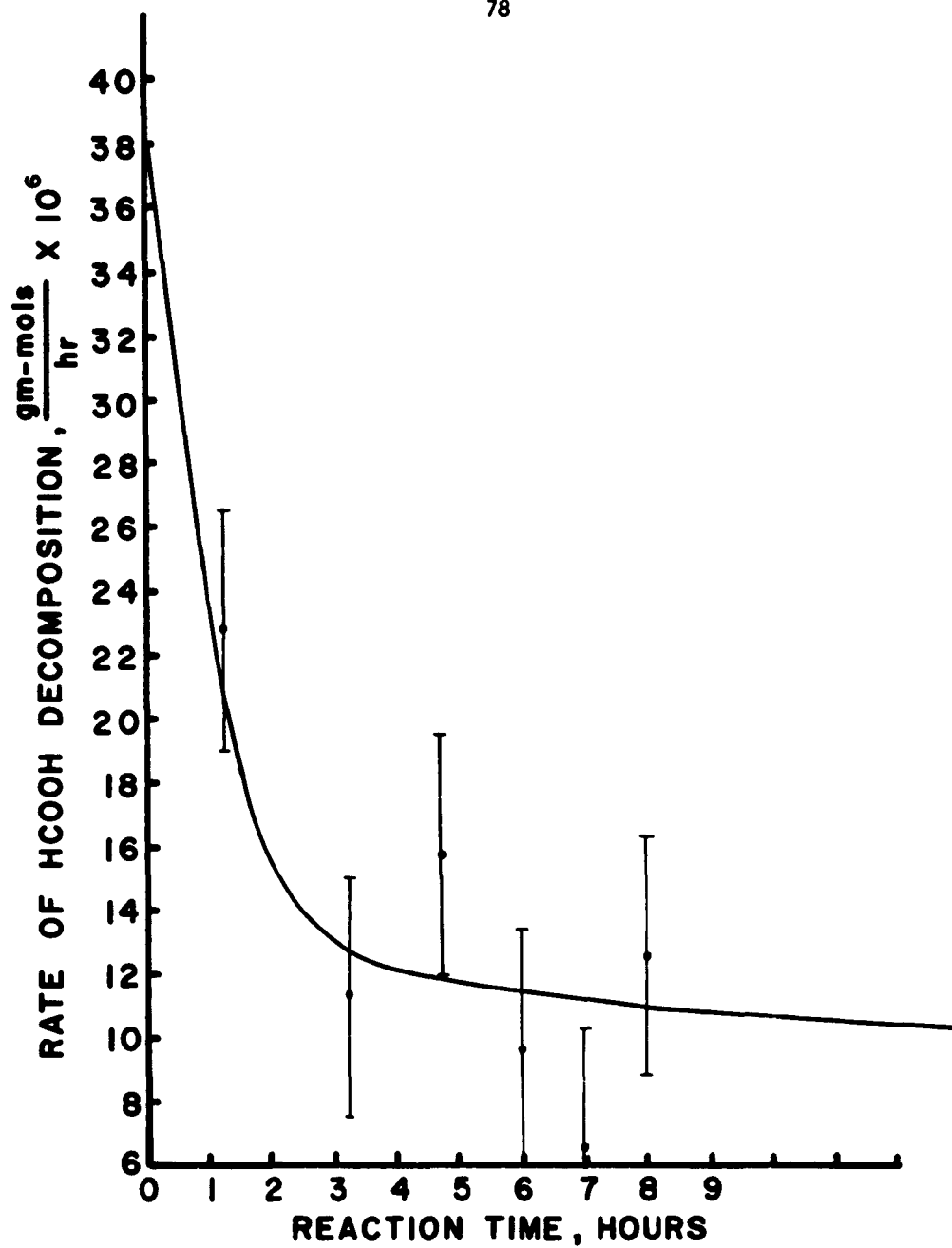
411 A
185.4 \pm 1.1 $^{\circ}$ C
40.17 cm 2
9.48 $\times 10^6$ \pm /cm 2

FIGURE 18



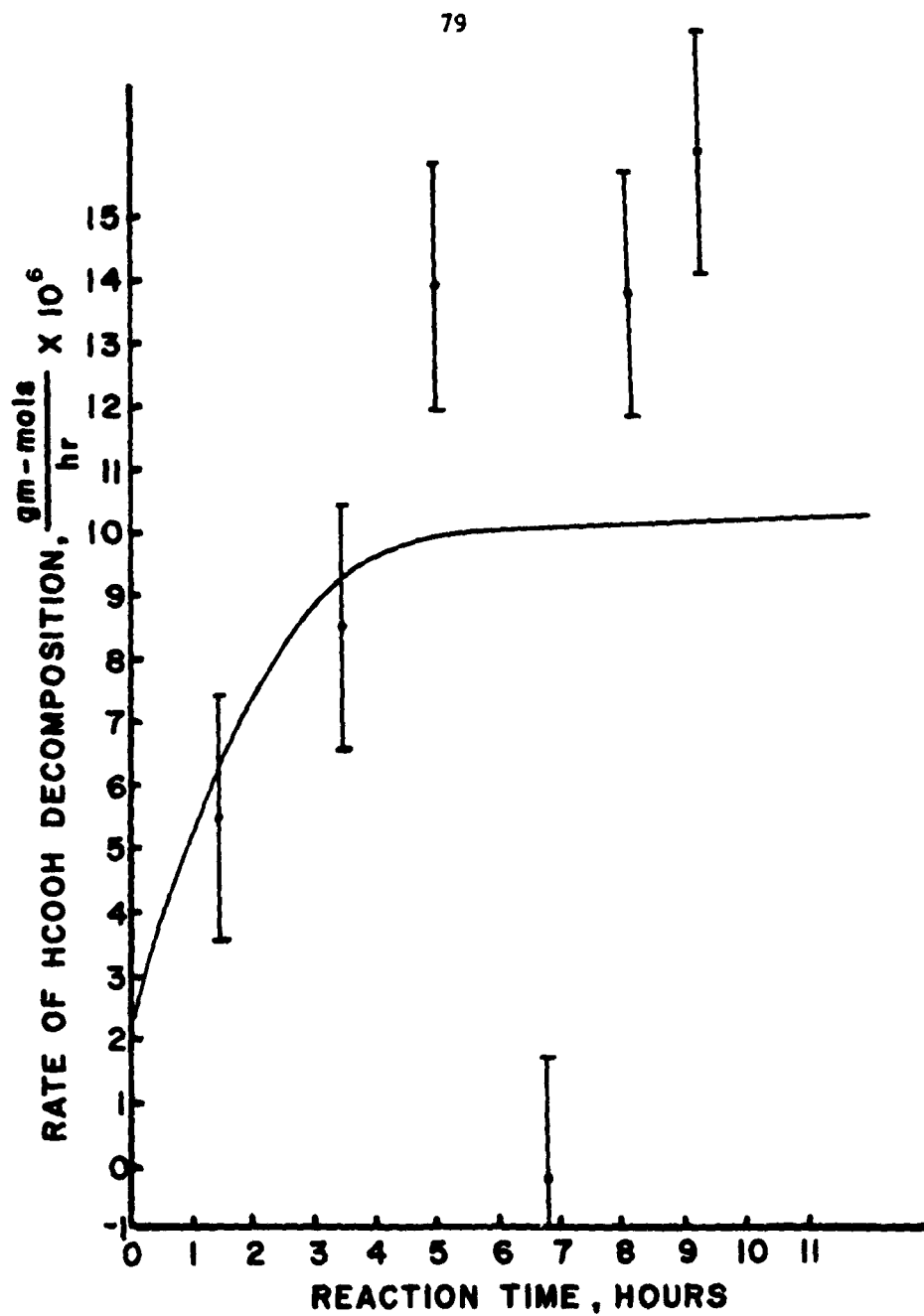
410 A
188.8° ± 1.1°C
36.44 cm²
1.57 × 10⁷ L/cm²

FIGURE 19



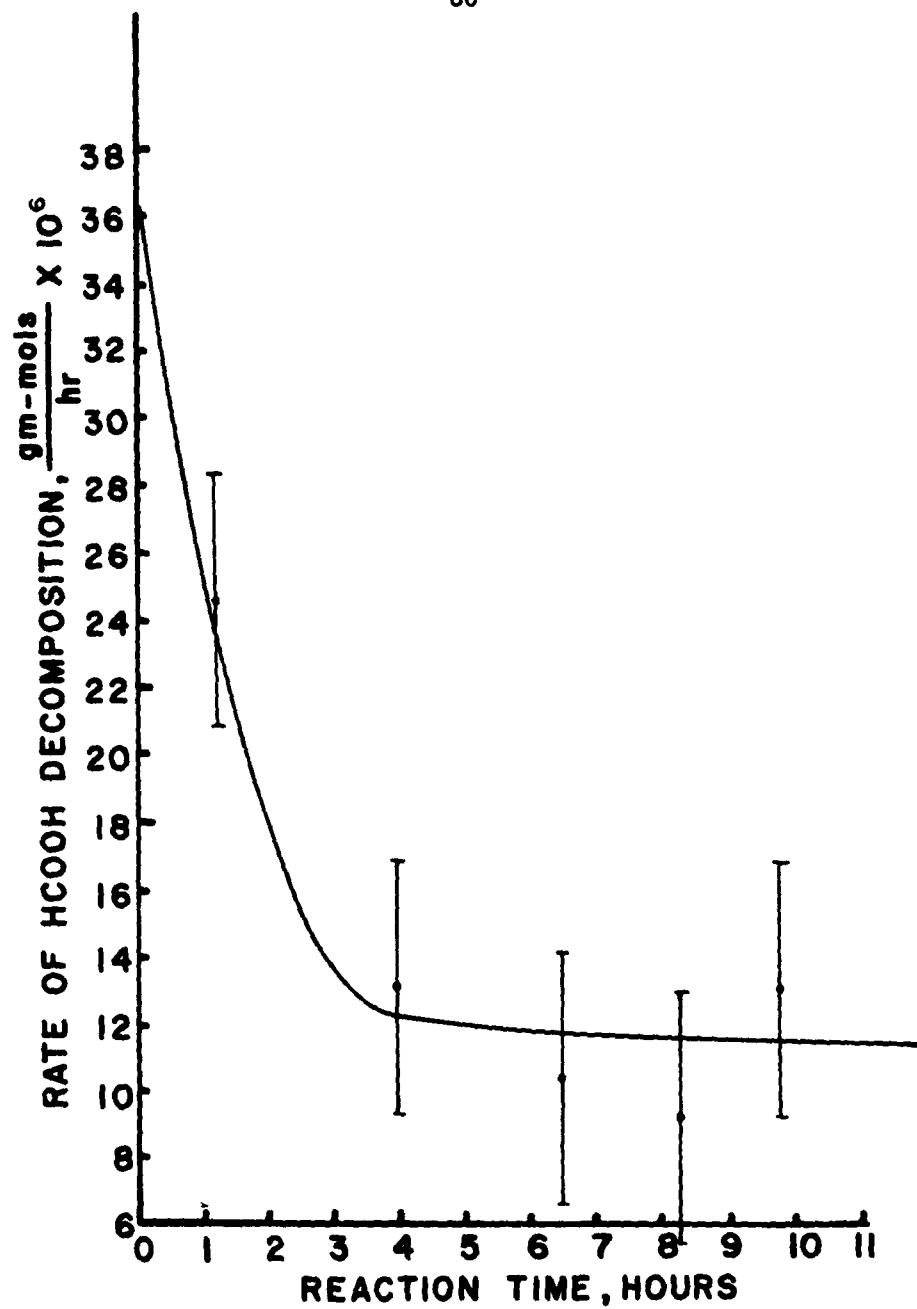
2410 A
187.7° ± 1.1°C
36.44 cm²
1.57 × 10⁷ 1/cm²

FIGURE 20



3410A
 175.0° ± 1.1° C
 36.44 cm²
 1.57 × 10⁷ ± /cm²

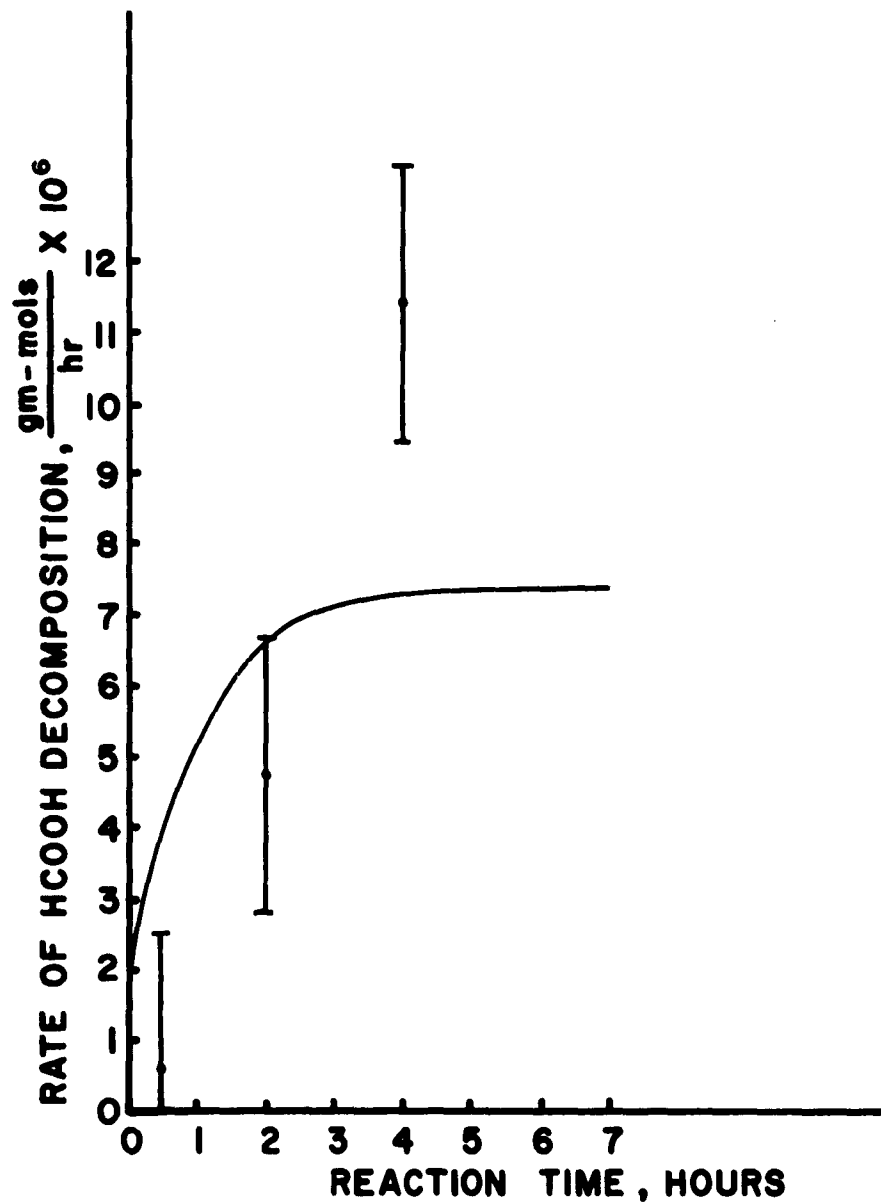
FIGURE 21



422 A
187.1° ± 1.1° C
50.1 cm²
1.0 × 10⁸ /cm²

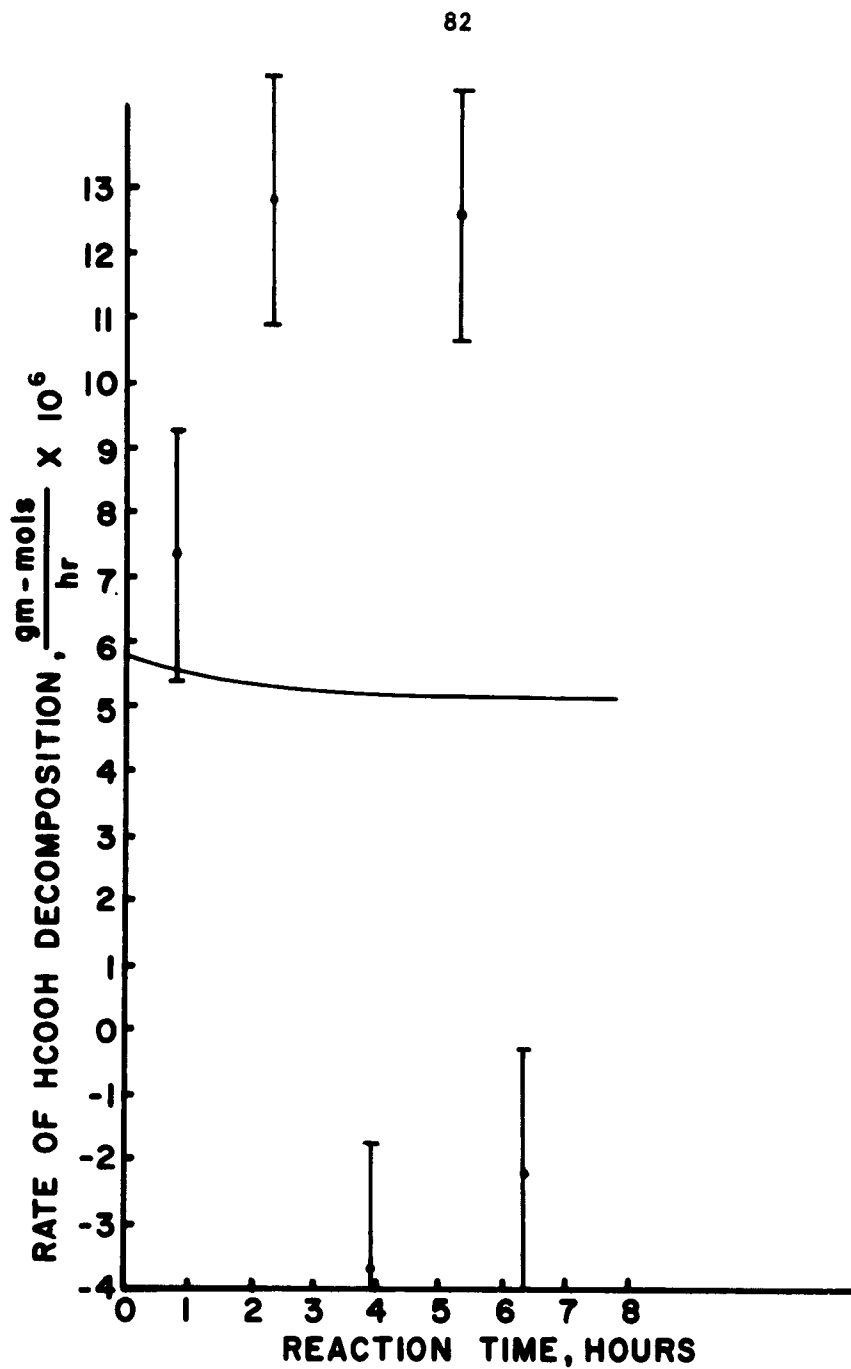
FIGURE 22

81



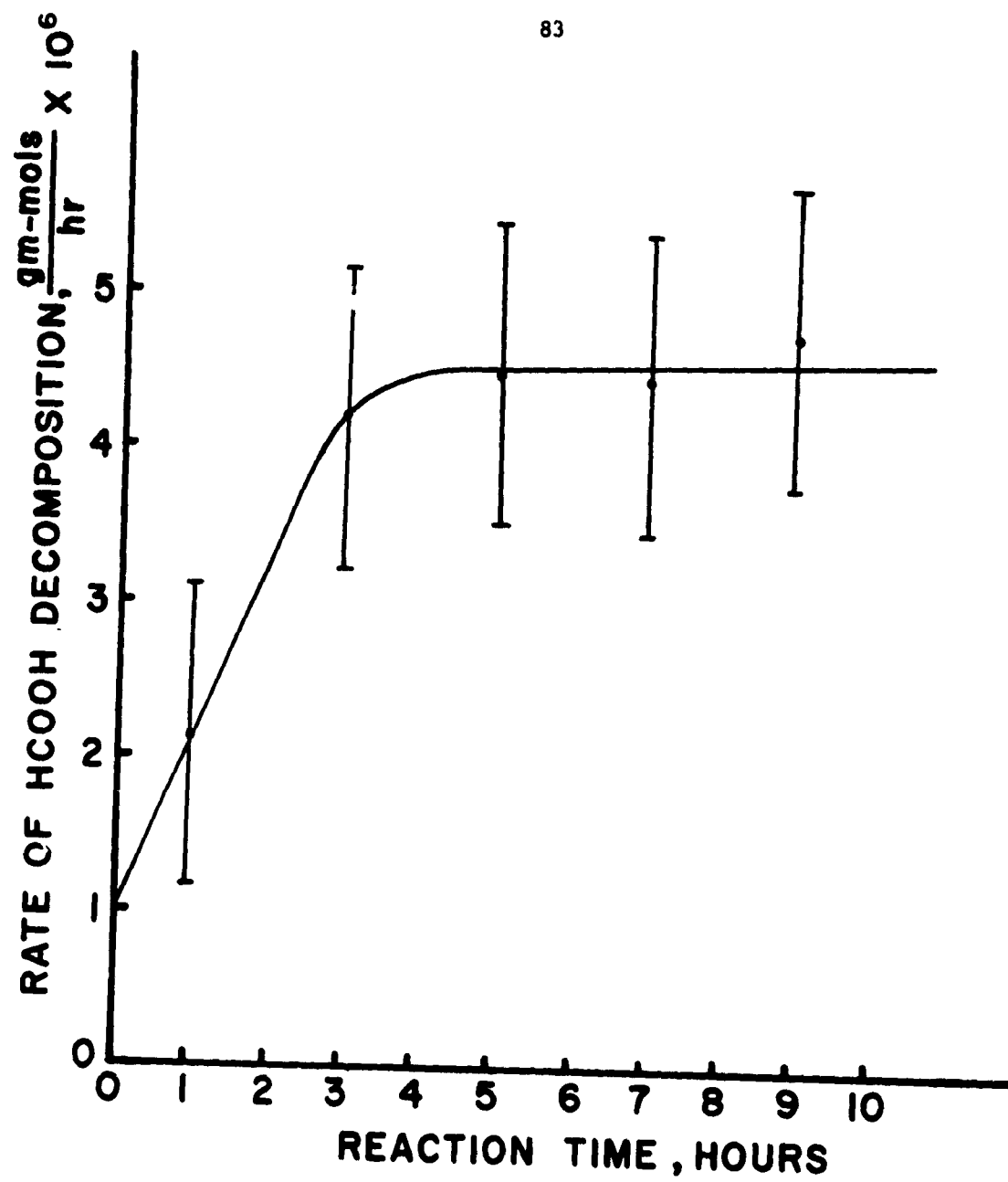
2422 A
175.5° ± 1.1°C
37.61 cm²
1.0 × 10⁸ /cm²

FIGURE 23



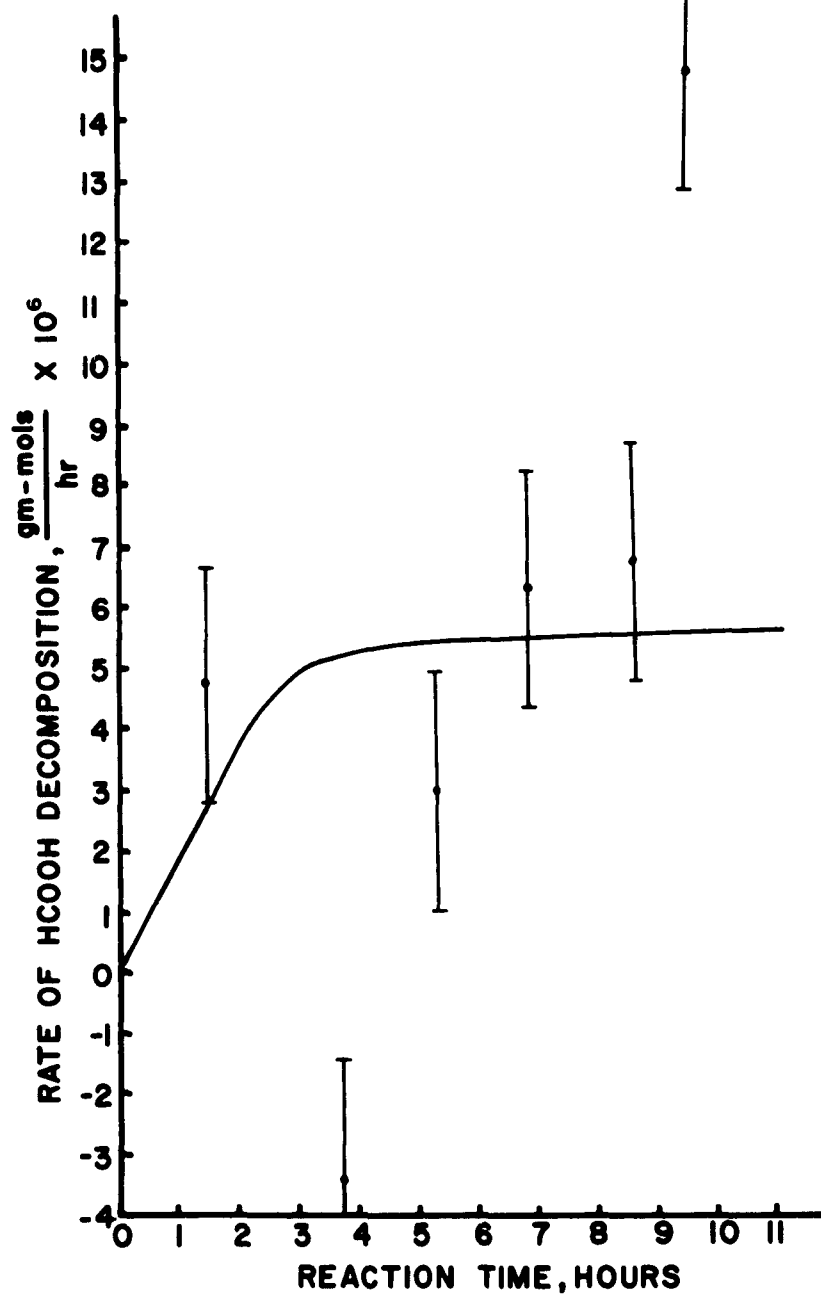
4422 A
 165.1° ± 1.1°C
 37.6l cm²
 1.0 × 10⁹ 1/cm²

FIGURE 24



#23
185.2° ± 1.1° C
UNCATALYZED

FIGURE 25



#24
176.0 \pm 1.1 $^{\circ}$ C
UNCATALYZED

FIGURE 26

Sample Data Sheet

Decomposition Formic Acid
Run 2410 A

Catalyst

Mass: 48.2957 grams
 Superficial surface area: 36.44 cm²
 Dislocation density: 1.57 x 10⁷ intersections/cm²

Feed to feed flask

Time: 0809
 Pressure before filling: 8.0 x 10⁻⁴ mm. Hg.
 Vacuum after filling: 687.0 mm. Hg.
 Temperature: 83.5°F
 Atmospheric pressure: 733.0 mm. Hg.

Feed (HCOOH) to reaction flask

Time: 1232
 Pressure before filling: 5.8 x 10⁻⁴ mm. Hg.
 Pressure after filling: 670.5 mm. Hg. (Vacuum)
 Temperature: 8.57 millivolts; reference 87°F
 Stirrer speed: 133 RPM
 Analysis:

	Peak height mv.	Attenuation	Time of efflux 25.0 ml.;sec.	Cell-column temp. °F
Air	0.23	X256	18.6	212
CO ₂	0.095	X512	18.1	212

Sample #1

Time: 1502
 Vacuum: 669.0 mm. Hg.
 Temperature: 8.54 mv; reference 90°F
 Analysis:

	Peak height mv.	Attenuation	Efflux time sec.	Cell-column temp. °F
Air	0.575	X32	18.6	212
CO ₂	0.58	X512	17.6	212

Sample #2

Time: 1632
 Vacuum: 673.0 mm. Hg.
 Temperature: 8.46 mv.; reference 91.5°F
 Analysis:

	Peak height	Attenuation	Efflux time
Air	0.78	X32	20.7
CO ₂	0.51	X256	19.2

86

Sample #3

Time: 1802
Vacuum: 728.0 mm. Hg.
Temperature: 8.52 mv.; reference 89°F
Analysis:

	Peak height	Attenuation	Efflux time
Air	0.94	X32	22.0
CO ₂	0.68	X256	21.6

Sample #4

Time: 1902
Vacuum: 680.5 mm. Hg.
Temperature: 8.56 mv.; reference 87.5°F
Analysis:

	Peak height	Attenuation	Efflux time
Air	0.50	X16	20.1
CO ₂	0.595	X256	19.5

Sample #5

Time: 2002
Vacuum: 684.5 mm. Hg.
Temperature: 8.63 mv.; reference 86°F
Analysis:

	Peak height	Attenuation	Efflux time
Air	1.035	X32	20.2
CO ₂	0.55	X256	19.4

Sample #6

Time: 2102
Vacuum: 687.5 mm. Hg.
Temperature: 8.67 mv.; reference 85°F
Analysis:

	Peak height	Attenuation	Efflux time
Air	0.49	X16	20.1
CO ₂	0.56	X256	19.4

Sample Calculation

Decomposition Formic Acid
Run 2410A

Sample #1

Normalized peak height for sample products (volume 38.01 ml.).

$$\text{Air: } \frac{60 \text{ sec/min (25.0 ml.)}}{18.6 \text{ sec (70 ml/min)}} [0.575 \text{ mv.}] = 0.663 \text{ mv}$$

$$7.4 \times 10^{-6} \text{ gm-mols (from calibration curve)}$$

$$\text{CO}_2: \frac{60 \text{ sec/min (25.0 ml.)}}{17.6 \text{ sec (70 ml/min)}} [0.58 \text{ mv.}] = 0.706 \text{ mv.}$$

$$7.22 \times 10^{-6} \text{ gm-mols (from calibration curve)}$$

CO: None detected

Materials present in reaction system (volume 541.7 ml.):

$$\text{Air: } \frac{7.4 \times 10^{-6} \text{ gm-mols (541.7 ml.)}}{38.0 \text{ ml.}} = 105.7 \times 10^{-6} \text{ gm-mols}$$

$$\text{CO}_2: \frac{7.22 \times 10^{-6} \text{ gm-mols (541.7 ml.)}}{38.0 \text{ ml.}} = 103.0 \times 10^{-6} \text{ gm-mols}$$

$$\text{H}_2: \text{ (Same as CO}_2\text{)} \quad 103.0 \times 10^{-6} \text{ gm-mols}$$

$$\text{HCOOH: By difference} \quad \underline{908.0 \times 10^{-6} \text{ gm-mols}}$$

$$\text{Total} = 1219.7 \times 10^{-6} \text{ gm-mols}$$

Pressure, calculated from analysis of Sample #1:

$$P = \frac{N R T}{V} = \frac{(1219.7 \times 10^{-6}) (3.46 \times 10^4) (830)}{541.7} = 64.0 \text{ mm. Hg.}$$

Pressure measured:

63.5 mm. Hg.

Fraction of reaction mixture lost in sampling and pressuring manometer

$$\frac{8.7 + 7.0 + 38.0}{488.0 + 8.7 + 7.0 + 38.0} = \frac{53.7}{541.7} = 0.0991$$

Quantities materials present at beginning of next reaction period:

$$\text{Air: } (0.9009) (105.7 \times 10^{-6}) = 95.1 \times 10^{-6} \text{ gm-mols}$$

$$\text{CO}_2: (0.9009) (103.0 \times 10^{-6}) = 92.7 \times 10^{-6}$$

$$\text{H}_2: (0.9009) (103.0 \times 10^{-6}) = 92.7 \times 10^{-6}$$

$$\text{HCOOH: } (0.9009) (908.0 \times 10^{-6}) = 817.0 \times 10^{-6}$$

Sample #2

Quantities materials present at end of sample period:

Air:	129.2×10^{-6} gm-mols
CO ₂ :	109.6×10^{-6}
H ₂ :	109.6×10^{-6}
HCOOH:	800.1×10^{-6}

Gm-mols of CO₂ produced = gm-mols of HCOOH decomposed

$$109.6 \times 10^{-6} - 92.7 \times 10^{-6} = 16.9 \times 10^{-6} \text{ gm-mols}$$

Elapsed time of reaction: 1.5 hours

Rate of decomposition:

$$\frac{16.9 \times 10^{-6} \text{ gm-mols}}{1.5 \text{ hr}} = 11.23 \times 10^{-6} \text{ gm-mols/hr}$$

TABLE 3
SUMMARY OF COMPUTED FORMIC ACID DECOMPOSITION RATES

Run No.	Temp. °C	Pressure mm Hg	Density $\frac{1}{\text{cm}^2} \times 10^{-7}$	Mass gms	Area 1 cm^2	Rate 2 $\times 10^6$	Rate 3 $\times 10^6$	Rate 4 $\times 10^8$	Rate 5 $\times 10^8$	Rate 6 $\times 10^8$	Rate 7 $\times 10^9$
524B	186.0	58.5-50.5	0.32	66.35	46.13	9.5	3.8	8.2	5.7	8.2	18.0
2524B	189.8	56.0-39.5	0.32	66.35	46.13	10.4	4.3	9.3	6.5	9.3	20.0
3524B	177.8	50.5-33.5	0.32	66.35	46.13	8.8	4.0	8.7	6.0	8.7	19.0
411A	185.4	40.0-37.0	1.00	49.75	40.17	6.8	1.2	3.0	2.4	2.6	5.7
410A	188.8	68.0-59.0	1.60	48.30	36.44	10.0	4.0	11.0	8.3	8.7	19.0
2410A	187.7	63.5-45.0	1.60	48.30	36.44	10.3	4.5	12.3	9.3	9.8	21.0
3410A	175.0	55.0-33.0	1.60	48.30	36.44	10.2	5.6	15.4	11.6	8.2	18.0
422A	187.1	68.0-54.0	10.00	57.82	50.10	11.4	5.6	11.2	9.7	7.2	16.0
2422A	175.5	29.5-27.0	10.00	43.40	37.61	7.3	2.7	7.2	6.2	4.6	10.0
4422A	165.0	20.0-11.0	10.00	43.40	37.61	5.2	1.4	3.7	3.2	2.4	5.2
238	185.2	67.0-37.0				4.7					
248	176.0	54.0-35.0				5.6					

Notes:

1. Superficial surface area.
2. Gross rate, gm-mol hr^{-1} , uncorrected for catalyzing influence of glass, tape.
3. Net rate, gm-mol hr^{-1} , promoted solely by silver catalyst.
4. Net rate, $\text{gm-mol hr}^{-1} \text{cm}^{-2}$, based on superficial area.
5. Net rate, $\text{gm-mol hr}^{-1} \text{gm}^{-1}$, based on mass of catalyst.
6. Net rate, $\text{gm-mol hr}^{-1} \text{cm}^{-2}$, based on hypothetical active area.
7. Net rate, $\text{gm-mol hr}^{-1} \text{cm}^{-2}$, based on hydrogen overpotential area.
8. Rate of decomposition as promoted by glass, tape, etc.

I
I
I

APPENDIX E
CHROMATOGRAPH CALIBRATION DATA

TABLE 4

CHROMATOGRAPH CALIBRATION DATA FOR
CARBON DIOXIDE & AIR*

Quantity gm-mols $\times 10^6$	Peak Height Millivolts	Attenuation	Carrier Flow ml/min
Carbon Dioxide			
3.80	0.14	512	81.1
4.13	0.16	512	82.0
4.55	0.23	512	86.6
4.90	0.26	512	70.5
5.35	0.31	512	81.0
5.82	0.42	512	82.1
6.40	0.58	512	70.2
7.56	0.60	256	64.8
7.65	0.42	256	81.5
8.25	0.69	256	76.5
8.46	0.70	256	81.0
9.00	0.80	256	63.0
9.67	0.44	128	82.7
9.79	0.56	128	70.3
11.10	0.56	128	87.0
10.60	0.66	128	72.8
11.60	0.83	128	74.2
12.50	0.75	128	73.3
14.20	0.53	64	73.0
16.10	0.65	64	84.0
18.10	0.83	64	85.2
20.00	0.53	32	79.0
22.10	0.66	32	79.6
24.20	0.77	32	80.8
27.20	0.95	32	77.5
30.20	0.55	16	80.1
34.30	0.59	16	93.7
39.60	0.73	16	83.0
Air			
5.9	0.90	64	68.3
6.1	0.89	64	74.2
6.4	0.49	32	79.7
6.8	0.99	64	71.7

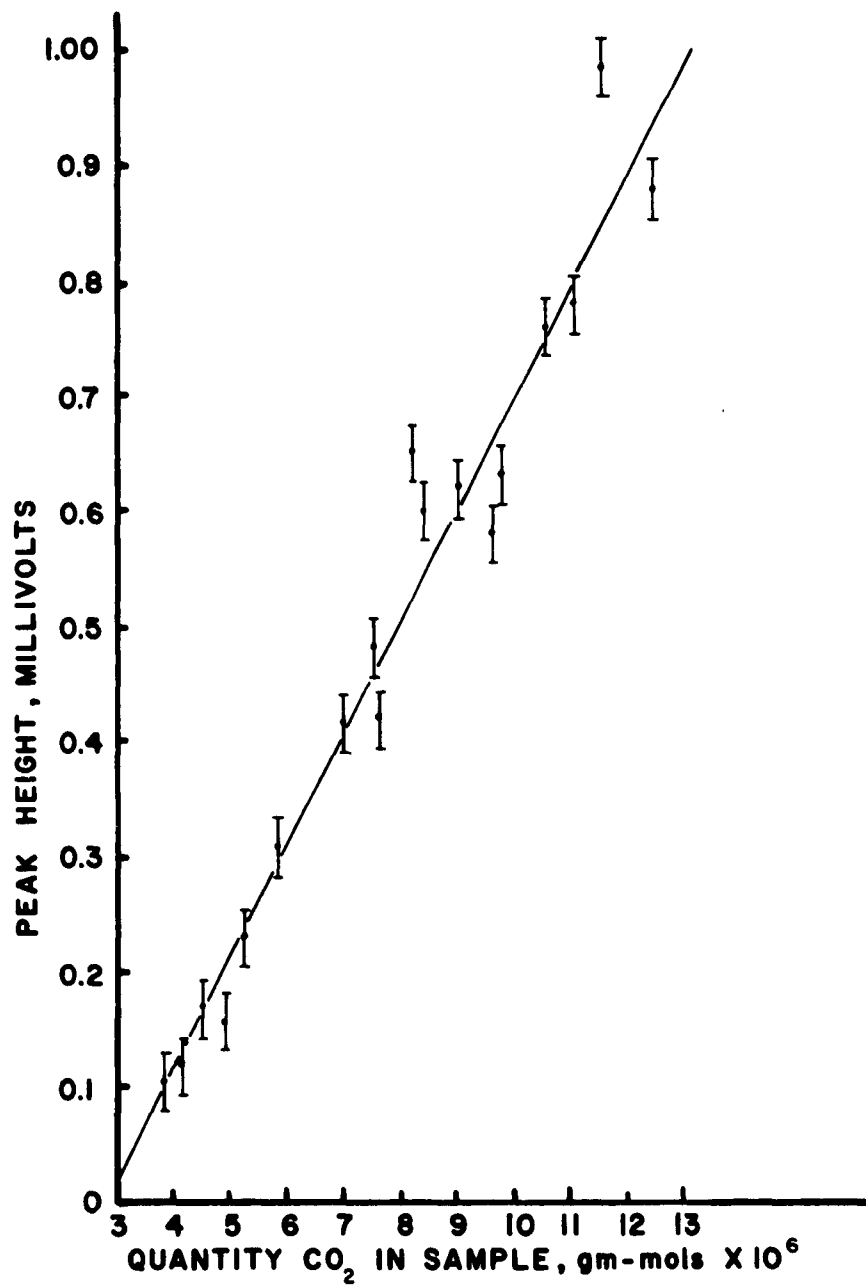
TABLE 4--Continued

Quantity gm-mols x 10 ⁶	Peak Height Millivolts	Attenuation	Carrier Flow ml/min
7.2	0.57	32	76.0
7.6	0.62	32	79.9
9.3	0.72	32	81.5
10.2	0.80	32	86.7
11.2	0.90	32	78.6
12.2	1.02	32	82.0
13.2	0.58	16	74.6
14.7	0.66	16	78.9
16.4	0.70	16	72.6
18.5	0.83	16	82.0
21.3	0.89	16	79.2
24.4	0.57	8	83.4
28.1	0.68	8	77.5
33.6	0.78	8	86.2
37.7	0.88	8	79.1
45.8	1.05	8	76.0

*Notes:

1. All calibration data were taken with the column and cell at a constant temperature of 212°F.
2. Observed peak height x [measured carrier flow/70] x attenuation factor = normalized peak height.
3. Attenuation factors were as follows:

Attenuation	Attenuation factor
8	1.7800
16	1.0000
32	0.5500
64	0.3310
128	0.1650
256	0.1260
512	0.0916



CHROMATOGRAPH CALIBRATION FOR CARBON
DIOXIDE

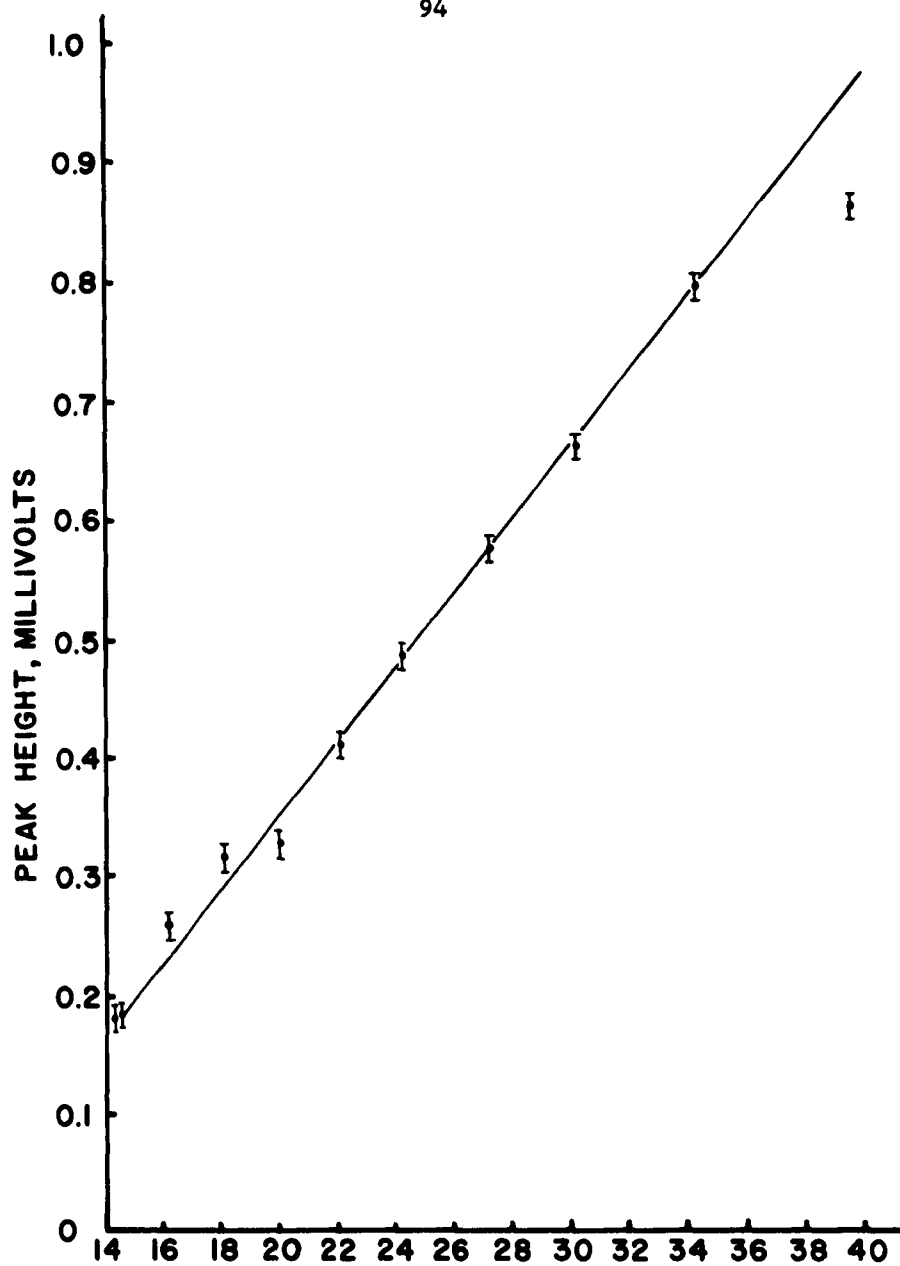
CARRIER FLOW 70 ± 0.5 ml/min

CELL & COLUMN TEMPERATURE $212 \pm 0.4^\circ$ F

COLUMN - 2 FT. ACTIVATED CHARCOAL

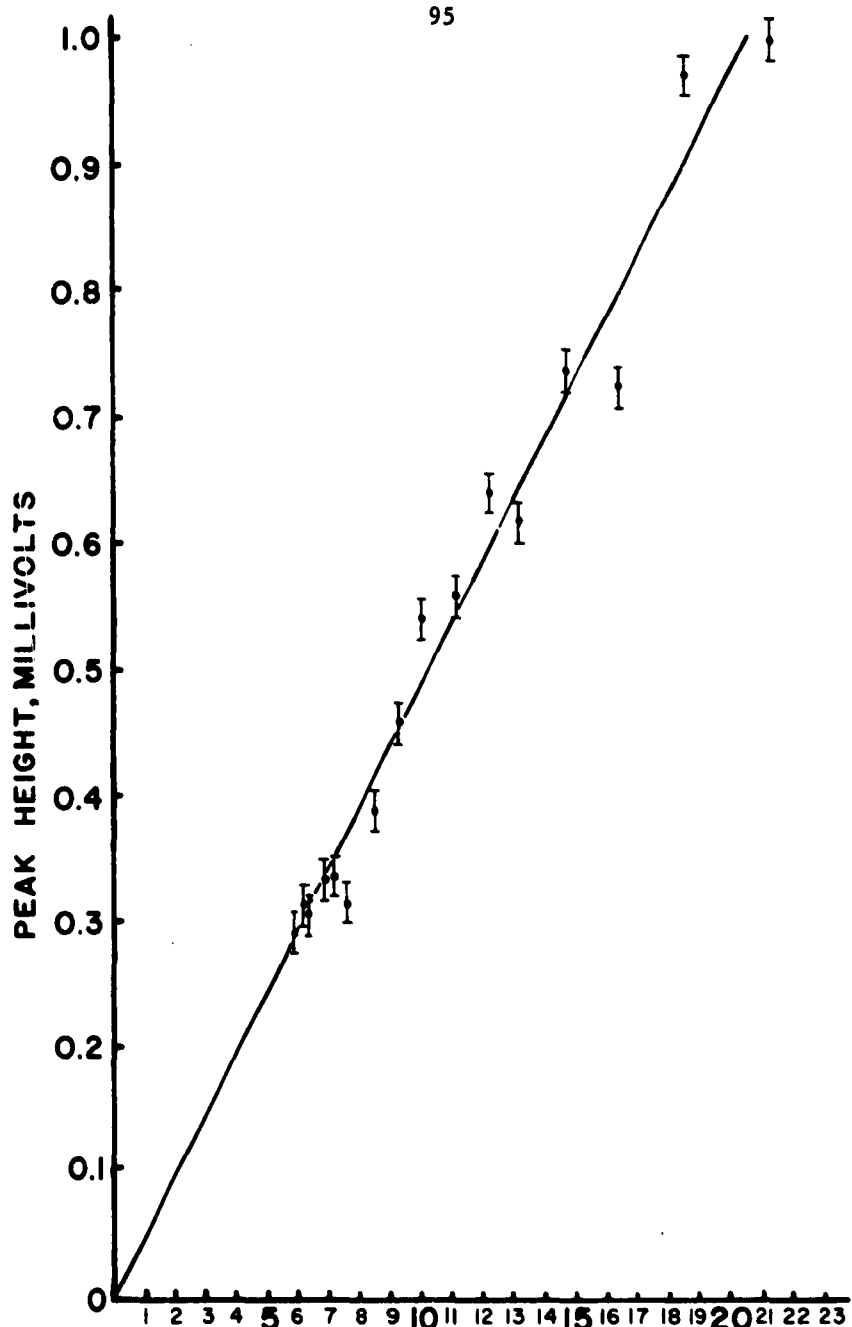
CELL CURRENT 10 ± 0.05 ma.

FIGURE 27



CHROMATOGRAPH CALIBRATION
FOR CARBON DIOXIDE
CARRIER FLOW 70 ± 0.5 ml/min
CELL & COLUMN TEMPERATURE $212 \pm 0.4^\circ$ F
COLUMN - 2 FT. ACTIVATED CHARCOAL
CELL CURRENT 10 ± 0.05 ma

FIGURE 28



QUANTITY AIR IN SAMPLE, gm-mols $\times 10^6$
CHROMATOGRAPH CALIBRATION FOR AIR
CARRIER FLOW 70 ± 0.5 ml/min
CELL & COLUMN TEMPERATURE $212 \pm 0.4^\circ$ F
COLUMN - 2 FT. ACTIVATED CHARCOAL
CELL CURRENT 10 ± 0.05 ma

FIGURE 29

I
I

APPENDIX F
EFFECT OF PRESSURE AND TEMPERATURE ON THE
DECOMPOSITION RATE OF FORMIC ACID

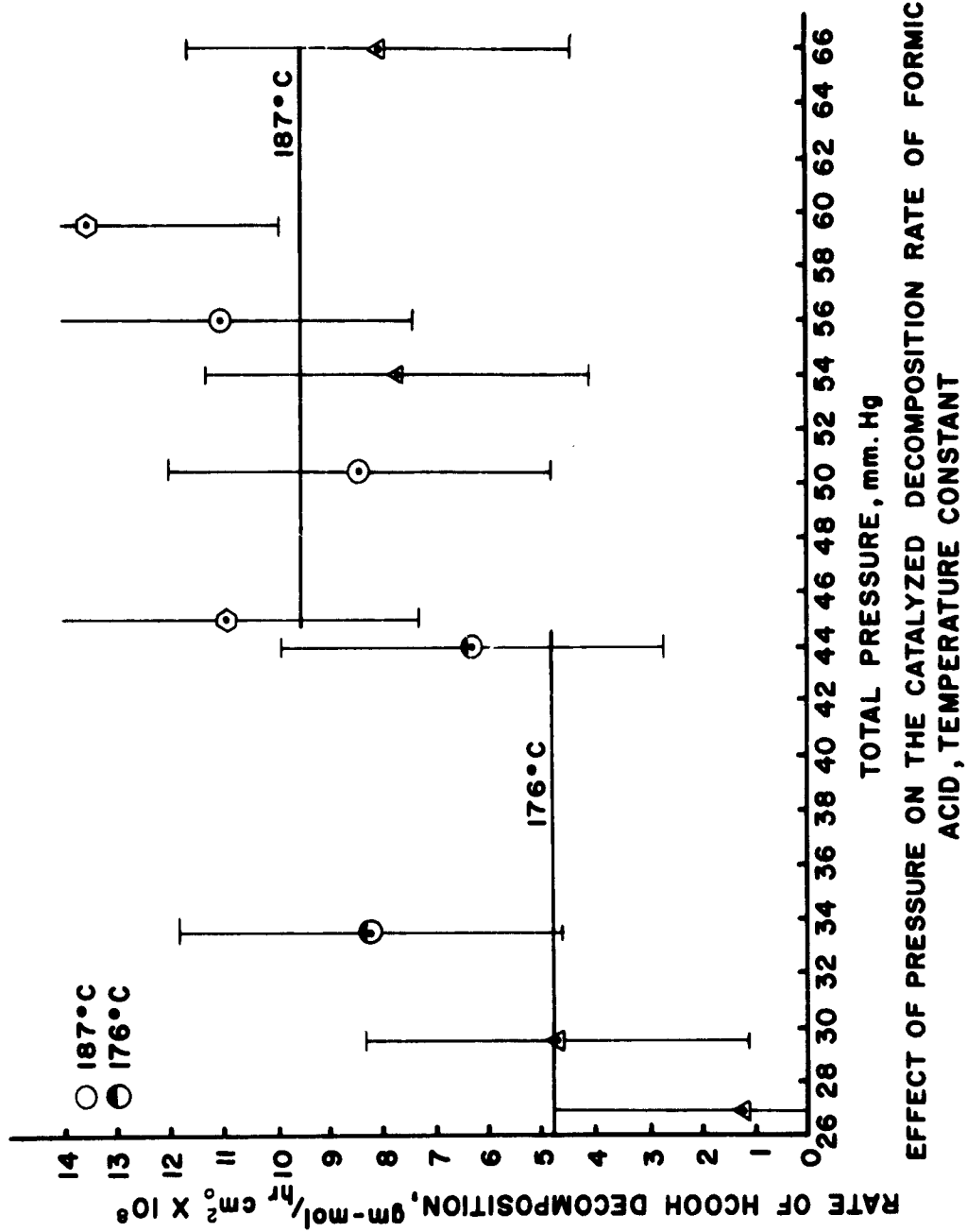
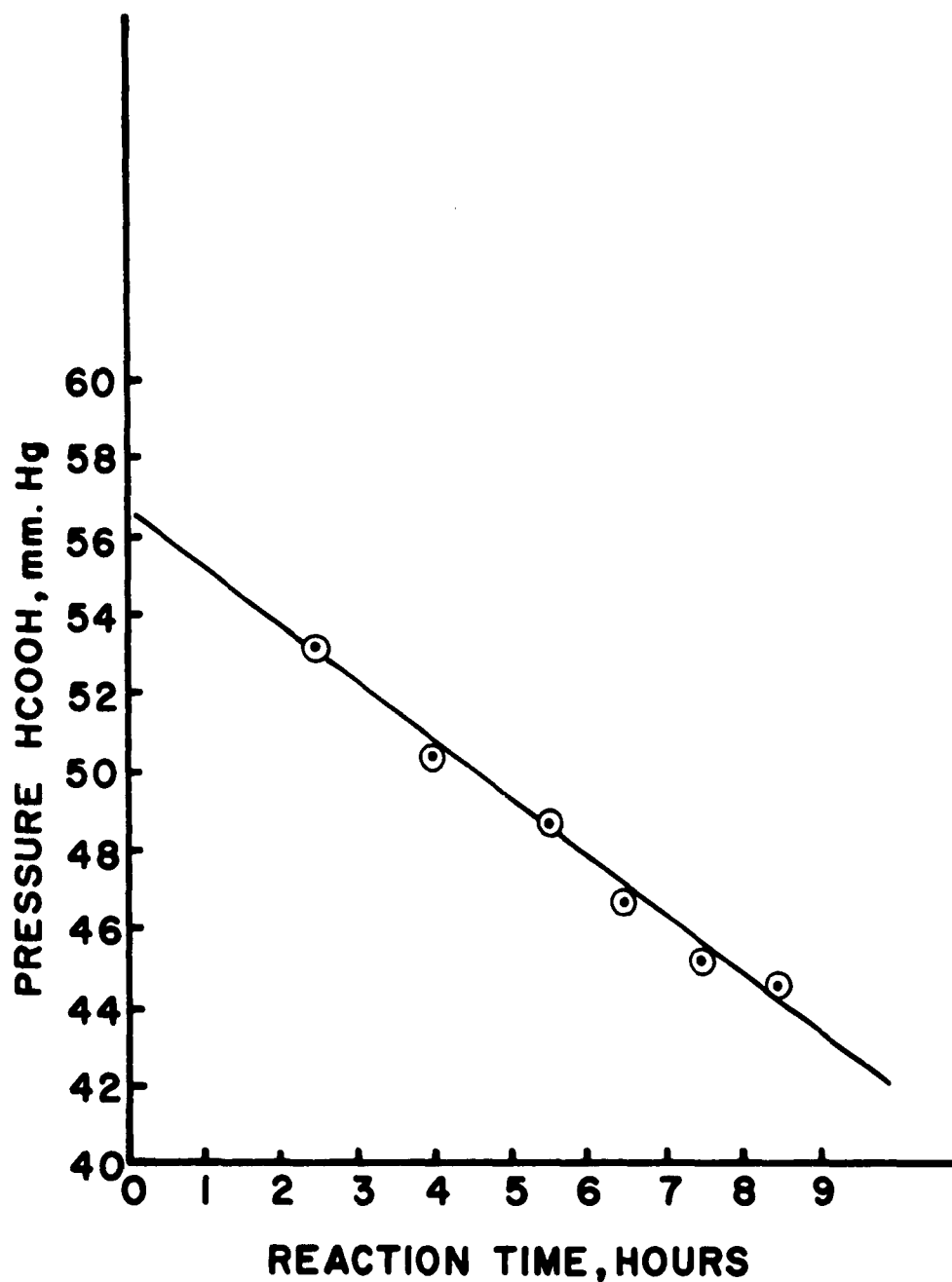
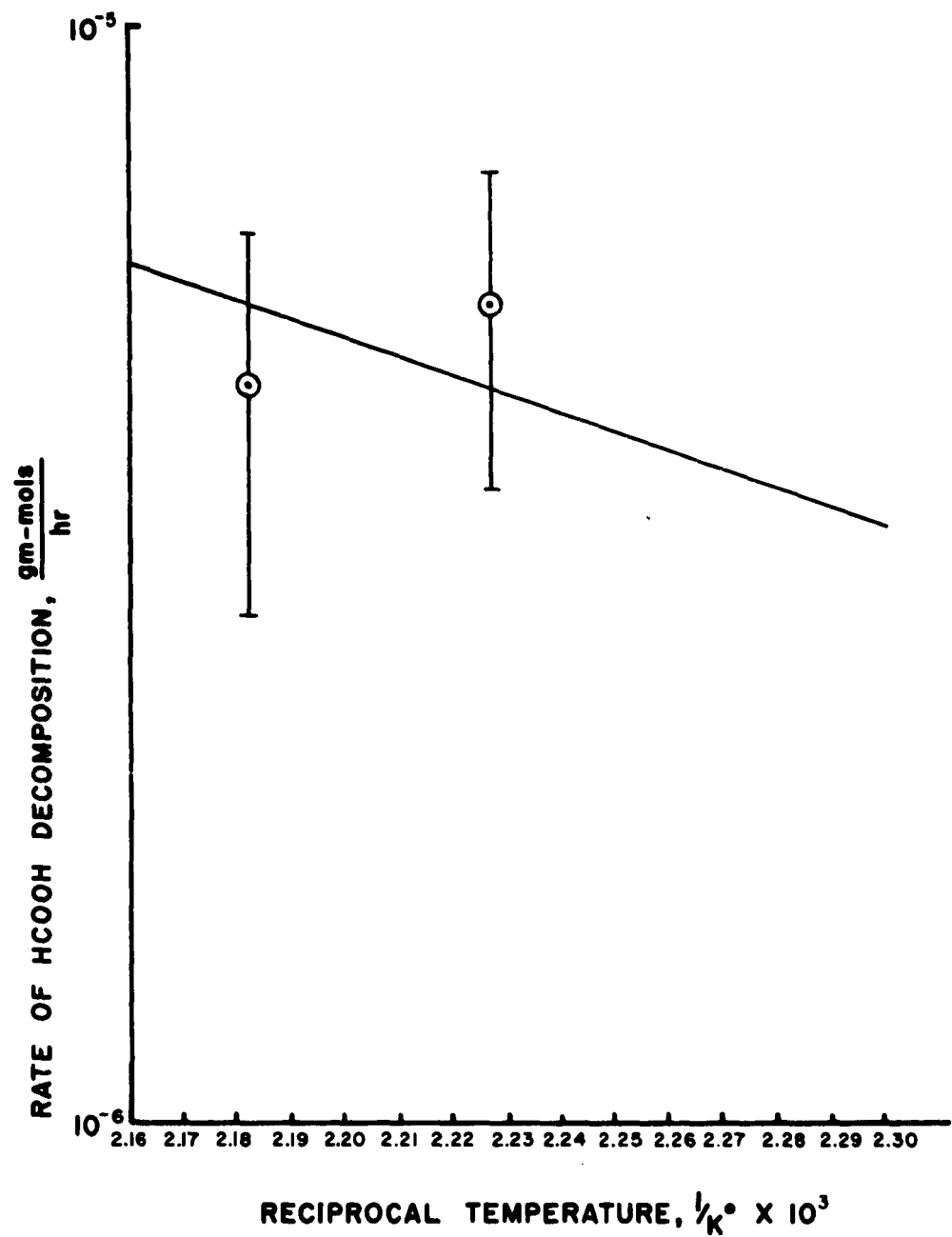


FIGURE 30



VARIATION OF PARTIAL PRESSURE OF FORMIC
ACID WITH REACTION TIME. RUN 2410 A

FIGURE 31



TEMPERATURE EFFECT ON THE UNCATALYZED DECOMPOSITION
RATE OF FORMIC ACID

FIGURE 32

APPENDIX G
ERRORS IN THE DISLOCATION DENSITY AND FORMIC ACID
DECOMPOSITION RATE MEASUREMENTS

TABLE 5

STANDARD DEVIATION DISLOCATION
DENSITY MEASUREMENTS

Specimen	Density $\frac{1}{\text{cm}^2}$	σ $\frac{1}{\text{cm}^2}$
524B	3.2×10^6	2.38×10^6
411A	1.0×10^7	0.95×10^7
410A	1.6×10^7	1.14×10^7

Note: Standard deviation, $\sigma_x = \sqrt{\sum(x_i - \bar{x})^2/n}$

TABLE 6

PROBABLE MEAN ERROR FORMIC ACID
RATE MEASUREMENTS (21)

Rate	Units	μ
Gross	gm-mol $\times 10^{-6}$ /hr	3.6×10^{-6}
Net	gm-mol $\times 10^{-8}$ /hr cm^2	$9.0 \times 10^{-8*}$
Net	gm-mol $\times 10^{-8}$ /hr cm^2 HOA	$1.6 \times 10^{-8*}$

Notes: Probable mean error, $\mu = 0.6745 \sqrt{\sum(r_e - r_d)^2/n}$

where r_e = experimental rate measurement

r_d = rate as shown on rate curve

n = number of measurements

*This presumes little or no error in superficial area or hydrogen overpotential area measurements.

APPENDIX H
CALCULATIONS FOR MASS TRANSFER AND
TEMPERATURE GRADIENTS IN THE
DECOMPOSITION REACTION

**MASS TRANSFER AND TEMPERATURE GRADIENTS
IN THE REACTION SYSTEM (29)**

Mass Transfer Gradient

$$\begin{aligned} \frac{\Delta P_A}{P_A} &= \frac{1}{\alpha} \left[\frac{\sqrt{a_p} r M_m P_f}{P_A \mu} \right] \left[\frac{\mu}{\rho D_{am}} \right]_f^{\frac{2}{3}} \left[\frac{\sqrt{a_p} G}{\mu} \right]^{-0.49} \\ &= \frac{1}{2.44} \left[\frac{0.067 (1.133 \times 10^{-4}) (44.4) (50)}{5.15 (2.42 \times 10^{-2}) (454)} \right] \\ &\quad \left[\frac{2.42 \times 10^{-2}}{(6.01 \times 10^{-3}) (10.78)} \right]^{\frac{2}{3}} \left[\frac{(0.067) (10.82)}{2.42 \times 10^{-2}} \right]^{-0.49} \\ &= 1.2 \times 10^{-5} \end{aligned}$$

At 50 mm Hg pressure and 370°F:

$$\underline{\Delta P} = P_A - P_{A_1} = 50 (1.2 \times 10^{-5}) = \underline{\underline{6 \times 10^{-4} \text{ mm Hg}}}$$

Temperature Gradient

$$\begin{aligned} \frac{\Delta T}{T} &= \frac{1}{\alpha'} \left[\frac{r \Delta H \sqrt{a_p}}{a_m \mu C_p T} \right] \left[\frac{C_p \mu}{k} \right]^{\frac{2}{3}} \left[\frac{\sqrt{a_p} G}{\mu} \right]^{n-1} \\ \Delta T &= \frac{1}{2.62} \left[\frac{(30.48) (1.1 \times 10^{-7}) (50.1) (-26.2) (2.04)}{57.82 (0.878) (0.0242) (0.2)} \right] \\ &\quad \left[\frac{(0.2) (0.0242)}{0.008} \right]^{\frac{2}{3}} \left[\frac{(0.067) (10.82)}{2.42 \times 10^{-2}} \right]^{-0.49} \\ \underline{\Delta T} &= t - t_1 = \underline{\underline{-0.0019^\circ F}} \end{aligned}$$

APPENDIX I
COMPUTED VALUES FOR THE DISLOCATION DENSITY
ENERGY AND THE ENERGY OF
PLASTIC DEFORMATION

TABLE 7

THEORETICAL ENERGY OF DISLOCATION DENSITIES*

Specimen	Depth cm	Dislocation Density $\frac{1}{\text{cm}^2} \times 10^{-7}$	Energy ergs/cm ² of (211) plane
524B	0.137	0.32	1.21×10^2
411A	0.118	1.00	2.62×10^2
410A	0.126	1.57	4.49×10^2
422A	0.110	10.00	21.30×10^2

*Calculated from Equation 5.

TABLE 8

APPROXIMATE ENERGY EXPENDED IN PLASTIC
DEFORMATION OF SAMPLES

Specimen	Bending Radius cm	Strain cm/cm	Energy Expended ergs/cm ² of (211) plane
411A	4.0	0.142	0.1×10^5
410A	1.32	0.256	0.4×10^5
422A	Cold rolled	0.928*	5.2×10^5

*Relation of shear strain and shear stress may not apply for strains greater than 0.5.

DISTRIBUTION LIST

Revised 16 February 1962

	No. Copies		No. Copies
Commanding Officer Office of Naval Research Branch Office The John Crerar Lib. Bldg. 86 E. Randolph Street Chicago 1, Illinois	(1)	Research Director Clothing & Organic Mat. Div. Quartermaster Res. & Engr. Com. U. S. Army Natick, Massachusetts	(1)
Commanding Officer Office of Naval Research Branch Office 346 Broadway New York 13, N. Y.	(1)	Air Force Office of Scientific Research (SRC-E) Washington 25, D. C.	(1)
Commanding Officer Office of Naval Research Branch Office 1030 E. Green Street Pasadena 1, California	(1)	Commanding Officer Diamond Ordnance Fuze Lab. Washington 25, D. C. Attn: Technical Informa- tion Office Branch 012	(1)
Commanding Officer Office of Naval Research Branch Office Box 39 Navy #100 Fleet P.O. New York, New York	(7)	Office, Chief of Research & Development Department of the Army Washington 25, D. C. Attn: Physical Sciences Division	(1)
Director, Naval Research Lab. Washington 25, D. C. Attn: Technical Infor- mation Officer Chemistry Div.	(6) (2)	Chief, Bureau of Ships Department of the Navy Washington 25, D. C. Attn: Code 342C	(2)
Chief of Naval Research Department of the Navy Washington 25, D. C. Attn: Code 425	(2)	Chief, Bureau of Naval Weapons Department of the Navy Washington 25, D. C. Attn: Technical Library Code RRMA-3	(3) (1)
DDR&E Technical Library Room 3C-128, The Pentagon Washington 25, D. C.	(1)	ASTIA Document Service Center Arlington Hall Station Arlington 12, Virginia	(10)
Technical Director Research & Engr. Div. Office of the Quarter- master General Department of the Army Washington 25, D. C.	(1)	Director of Research U.S. Army Signal Res. & Development Laboratory Fort Monmouth, N. J.	(1)

Naval Radiological Defense Laboratory San Francisco 24, Cal. Attn: Technical Library	(1)	Dr. J. H. Schulman Dept. of Metallurgy Columbia University New York, New York	(1)
Naval Ordnance Test Station China Lake, California Attn: Head, Chem. Div.	(1)	Dr. E. S. Machlin Dept. of Metallurgy Columbia University New York, New York	(1)
Commanding Officer Army Research Office Box CM, Duke Station Durham, North Carolina Attn: Scientific Synthesis Office	(1)	Dr. J. H. Johnston Minneapolis-Honeywell Res. Cen. Hopkins, Minnesota	(1)
Brookhaven National Lab. Chemistry Department Upton, New York	(1)	Dr. J. Hirth Dept. of Metallurgical Engr. Carnegie Institute of Tech. Pittsburgh, Penn.	(1)
Atomic Energy Commission Division of Research Chemistry Programs Washington 25, D. C.	(1)	Dr. E. R. Parker Div. of Engineering Res. University of California Berkeley, California	(1)
Atomic Energy Commission Div. of Technical Information Extension Post Office Box 62 Oak Ridge, Tennessee	(1)	Dr. L. Himmel Div. of Engineering Res. University of California Berkeley, California	(1)
U.S. Army Chemical Res. & Development Lab. Technical Library Army Chemical Center, Md.	(1)	Dr. A. R. Westwood RIAS 7212 Bellona Avenue Baltimore 12, Maryland	(1)
Office of Technical Services Department of Commerce Washington 25, D. C.	(1)	Dr. N. Hackerman Department of Chemistry University of Texas Austin, Texas	(1)
Chief of Naval Research Department of the Navy Washington 25, D. C. Attn: Code 423	(1)	Dr. N. Cabrera Department of Physics University of Virginia Charlottesville, Va.	(1)
ONR Resident Representative University of Texas Post Office Box 7786 Austin 12, Texas	(1)	Dr. J. H. Holloman General Electric Res. Lab. Box 1088 Schenectady, New York	(1)
		Dr. R. Sosnovsky Armour Research Foundation Technology Center Chicago 16, Illinois	(1)

Dr. M. R. Achter
Code 6340
Naval Research Laboratory
Washington 25, D. C. (1)

Dr. Peter Gibbs
Department of Physics
University of Utah
Salt Lake City 12, Utah (1)

Dr. A. T. Gwathmey
Department of Chemistry
University of Virginia
Charlottesville, Va. (1)

Lewis Research Center
21000 Brookpark Road
Cleveland 35, Ohio
Attn: Chief Librarian (1)

Dr. P. W. Selwood
Department of Chemistry
Northwestern University
Evanston, Illinois (1)

Mr. P. W. Ladd
NASA Lewis Research Center
Cleveland, Ohio (1)

Dr. E. Banks
Department of Chemistry
Polytechnic Institute of
Brooklyn
Brooklyn 1, New York (1)

Dr. George J. Janz
Department of Chemistry
Rensselaer Polytechnic Inst.
Troy, New York (1)

Dr. E. Yeager
Department of Chemistry
Western Reserve University
Cleveland, Ohio (1)

Dr. G. Barth-Wehrenalp, Dir.
Inorganic Research Dept.
Pennsalt Chemicals Corp.
Post Office Box 4388
Philadelphia 18, Penna. (2)

Dr. M. S. Cohen, Chief
Propellants Synthesis Sec.
Reaction Motors Division
Denville, New Jersey (1)

Dr. A. M. Zwickel
Department of Chemistry
Clark University
Worcester, Mass. (1)